Received: 9 November 2021 | Revised: 19 May 2022 | Accepted: 6 July 2022 | Published on: 24 July 2022

DOI: 10.1002/joc.7797

RESEARCH ARTICLE

International Journal of Climatology RMetS

Tropical cyclone activity in the Solomon Islands region: Climatology, variability, and trends

Alick Haruhiru[1] | **Savin S. Chand**[1] | **Christopher Turville**[1] | **Hamish Ramsay**[2]

[1]Institute of Innovation, Science and Sustainability, Federation University Australia, Ballarat, Victoria, Australia

[2]CSIRO Oceans and Atmosphere, Aspendale, Victoria, Australia

Correspondence
Alick Haruhiru, Institute of Innovation, Science and Sustainability, Federation University Australia, Mt Helen Campus, Ballarat, Vic 3350, Australia.
Email: a.haruhiru@federation.edu.au or alikiey@gmail.com

Funding information
Department of Foreign Affairs and Trade, Australian Government, Grant/Award Number: Australian Award Scholarship

Abstract

This study examines the climatology, variability, and trends of tropical cyclones (TCs) affecting the Solomon Islands (SI) territory, in the wider southwest Pacific (SWP), using the South Pacific Enhanced Archive for Tropical Cyclones (SPEArTC) database. During the period 1969/1970–2018/2019, 168 TCs were recorded in the SI territory. A cluster analysis is used to objectively partition these tracks into three clusters of similar TC trajectories to obtain better insights into the effects of natural climate variability, particularly due to the El Niño–Southern Oscillation (ENSO) phenomenon, which otherwise is not very apparent for TCs when considered collectively in the SI region. We find that TCs in clusters 1 and 3 show enhanced activity during El Niño phase, whereas TCs in cluster 2 are enhanced during La Niña and neutral phases. In addition to being modulated by ENSO, TCs in clusters 2 and 3 show statistically significant modulation at an intraseasonal timescale due to the Madden–Julian Oscillation (MJO) phenomenon. There are also some indications through sophisticated Bayesian modelling that TCs in clusters 2 and 3 are slightly influenced by the Interdecadal Pacific Oscillation (IPO). These results can have substantial implications for cluster-specific development of TC prediction schemes for the SI region.

KEYWORDS

El Niño–Southern Oscillation, Madden–Julian Oscillation, tropical cyclones

1 | INTRODUCTION

The influence of the El Niño–Southern Oscillation (ENSO)—a major driver of interannual climate variability—on tropical cyclone (TC) activity in the wider southwest Pacific (SWP) region (0–35°S, 135°E–120°W; Figure 1a) has been the subject of a widespread investigations in the past (Hastings, 1990; Kuleshov *et al.*, 2009; Dowdy *et al.*, 2012; Chand *et al.*, 2020). During El Niño events, TC activity is enhanced around the east of 165°E, extending to the Cook Islands and French Polynesia, while simultaneously low TC occurrence dominates the western part of the Pacific around the Coral Sea and Australian regions (Basher and Zheng, 1995; Chand *et al.*, 2019). In contrast, the reverse happens during La Niña years when TC activity is displaced westward into the Coral Sea and Australian regions with relatively low TC activity occurs over the east of ~165°E (Dowdy *et al.*, 2012; Ramsay *et al.*, 2014). However, the ENSO–TC relationship in the subregion 5°–15°S and 155°–170°E of the broader

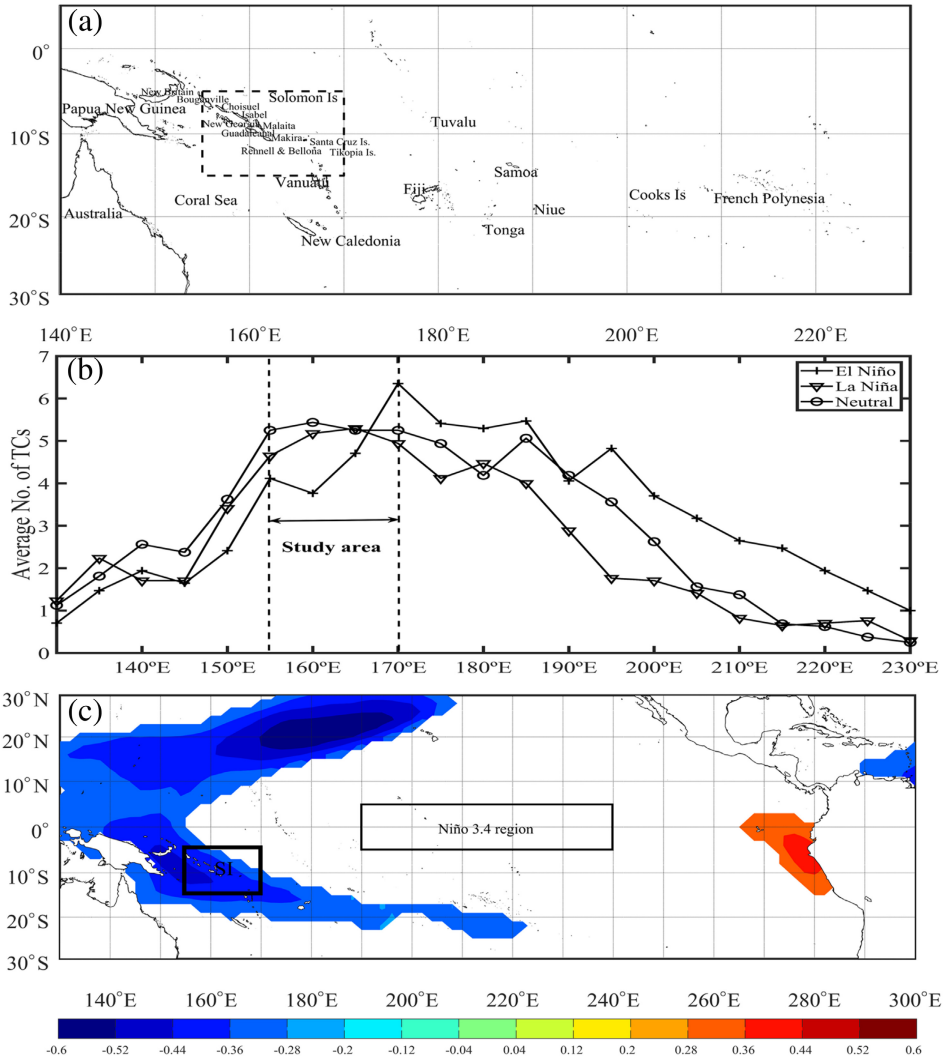

FIGURE 1 (a) Map of Southwest Pacific region, showing Solomon Islands territory (dashed rectangular region), (b) average number of TCs making longitudinal crossing during various ENSO phases at every 5°, and (c) correlation between total number of observed TCs in SI territory with the Extended Reconstructed Sea Surface Temperature, Version 5 (ERSSTv5) during the months November–April from 1969/1970 to 2018/2019 [Colour figure can be viewed at wileyonlinelibrary.com]

SWP, spanning the Solomon Islands (SI) where the spatial phase change of ENSO occurs (i.e., around ~165°–170°E; Figure 1b), is poorly defined. Consequently, this can have considerable repercussions on cyclone predictability around the SI territories. Indeed, the present-day statistical models utilized by the Solomon Islands Meteorological Service (SIMS) for seasonal prediction of TC activity over the region suffer from substantial limitations (Director of SIMS, 2018, personal communication). These models use ENSO indices as the key predictors of TCs when clearly, for example, the overall seasonal TC numbers in the SI territory are not well correlated with ENSO indices (Figure 1c). To isolate the predictable aspects of TCs impacting that region, the probabilistic behaviour of TC trajectories needs to be better understood. In this paper, our main emphasis is to objectively separate TC tracks over the SI territory into specific clusters (or "regimes") of similar spatial characteristics and then examine the influence of various climate drivers on each cluster separately, with the emphasis on ENSO. Past studies have revealed that understanding TC behaviour in terms of specific regimes can have implications on local-scale risk assessments and improved seasonal predictability of TCs (Hess *et al.*, 1995; Camargo *et al.*, 2007a; Choi *et al.*, 2016; Magee *et al.*, 2020).

A well-known climatic feature in the SWP, which spans the SI territory, is the South Pacific Convergence Zone (SPCZ) where TCs are frequently spawned (e.g., Chand *et al.*, 2020). The SPCZ is characterized by an intense convective precipitation, band of high cloudiness, and low-level convergence stretching northwest–southeast, diagonally from near the SI (0°, 150°E) towards French Polynesia (30°S, 120°W). The western tropical portion of the climate feature lies over the West Pacific Warm Pool, which is a region of relatively warmer sea surface temperature (SST) while the eastern portion undertakes regular mid-latitude interactions that contribute to its diagonal orientation (e.g., Vincent, 1994). The SPCZ is well defined during the months of December–February,

and so is responsible for significant convective activities during these months; it is weaker and less defined in June–August (Vincent, 1994). Moreover, the interannual variability of the SPCZ is strongly influenced by the impact of ENSO such that the mean position of the SPCZ moves northeastward during El Niño and southwestward during La Niña events (Vincent, 1994; Vincent *et al.*, 2011; Widlansky *et al.*, 2011). Consequently, TC numbers in the broader South Pacific (SP) are also influenced by the associated shifts in the mean location of the SPCZ. For example, a southwestward shift in the SPCZ location during La Niña creates more favourable large-scale environmental conditions (such as reduced environmental vertical wind shear, increased cyclonic relative vorticity, etc.) for TC genesis in the far western SP region. On the contrary, a northeastward shift in the SPCZ during El Niño events corresponds to more TCs forming around the central and eastern part of the SP region (e.g., Kuleshov *et al.*, 2009; Dowdy *et al.*, 2012). Additionally, it is worth noting that TC activity in the SWP also appears to have connections with SST variability in regions outside of the SWP such as with the Indian Ocean SST variability (Magee and Verdon-Kidd, 2018).

Elsewhere around the globe, extensive work has been done over the past several decades to understand the effect of ENSO on TC activity (e.g., Felton *et al.*, 2013; Jien *et al.*, 2015; Patricola *et al.*, 2018; Lin *et al.*, 2020). ENSO significantly alters the large-scale environmental conditions globally, thus profoundly influencing global TC activity (Ramsay, 2017). For example, over the western North Pacific, long-lived TCs are more prominent during El Niño years as more TCs tend to form near the International Dateline (IDL) and track northwestward, as opposed to La Niña years when TCs tend to form more towards the Asian coast (e.g., the South China Sea region) with a significant role played by both dynamical and thermodynamical large-scale factors (Chan, 1985; Liu *et al.*, 2019). Similarly, in the central eastern North Pacific, El Niño shifts TCs away from the Mexican coast and towards the IDL (e.g., Camargo *et al.*, 2008; Jien *et al.*, 2015; Krishnamurthy *et al.*, 2016). Over the North Atlantic, TC activity is significantly suppressed during El Niño years, with a reduction of landfall along the U.S. coastline, while TC activity and U.S. landfall likelihood are increased during La Niña (e.g., Krishnamurthy *et al.*, 2016). In the South Indian Ocean, TC activity is enhanced west of 75°E, extending westward as far as the African east coast in El Niño years. The opposite happens during La Niña years when TC activity is enhanced east of 75°E, extending into the Australian region (Kuleshov *et al.*, 2009).

Another type of El Niño (referred to as the "El Niño Modoki") is observed over the recent decades. Unlike the traditional El Niño, El Niño Modoki is confined more to the central tropical Pacific region (e.g., Ashok *et al.*, 2007). This "flavour" of ENSO has also been found to influence TC activity globally (e.g., Kim *et al.*, 2009; Chen and Tam, 2010; Chen, 2011; Hong *et al.*, 2011) and in the SWP region (e.g., Chand *et al.*, 2013a; Ramsay *et al.*, 2014; Magee *et al.*, 2017). For the SWP region, Chand *et al.* (2013a, 2013b) identified four ENSO regimes with different impacts on cyclone genesis positions and frequency. Two of these regimes were linked with the conventional El Niño and La Niña events while the rest, which they termed "positive-neutral" and "negative-neutral," demonstrated Modoki-type patterns. Magee *et al.* (2017) reported latitudinal shifts in the mean location of the SWP TC genesis positions, with a northward displacement during El Niño Modoki and a southward displacement during La Niña Modoki phase. Additionally, TC activity in the SWP also shows a substantial "ENSO-like" variability but at interdecadal timescale linked to the Interdecadal Pacific Oscillation (IPO) (e.g., Magee *et al.*, 2017; Sharma *et al.*, 2020). IPO is often described as having a related climate variability pattern as ENSO in the tropical Pacific but at the decadal timescale (Mantua *et al.*, 1997; Zhang *et al.*, 1997; Newman *et al.*, 2016). Indeed, Salinger *et al.* (2001) has reported that IPO has a significant influence on the SWP climate trends on decadal timescale and its association with ENSO teleconnections. For example, the sudden shift from negative to positive IPO during mid-1970s was connected with a shift to an El Niño dominated years whereas the shift to a negative IPO after around the year 2000 was connected with La Niña dominated years. Magee *et al.* (2017) has indicated that the synergetic match of positive IPO and El Niño would enhance the northeast shift of TC genesis locations in the SWP, whereas the opposite phases (i.e., negative IPO and La Niña) would enhance the southwest shift.

At the intraseasonal timescale, the Madden–Julian Oscillation (MJO) phenomenon has a substantial influence on regional TC activity in the SWP (Kiladis *et al.*, 2005; Zhang, 2013). The MJO is a meteorological occurrence that has 30–90 days of unstable atmospheric conditions (e.g., rainfall, convective clouds, and winds) that propagates eastwards across the Tropics, and hence can substantially affect weather patterns over the wider tropical South Pacific Ocean (SPO), extending farther east to ~80°W (Hendon and Salby, 1994). The MJO phases can be divided into two general groups, namely the enhanced convective group (comprises active phases of the MJO or wetter weather conditions) and a suppressed convective group (inactive phases or drier weather conditions) (Zhang, 2005). Diamond and Renwick (2015) showed that TC frequency in the SP region is suppressed

by ~17% during inactive phases of the MJO in the region (i.e., phases 2–3) while TC activity is enhanced by ~36.7% during the active phases (i.e., phases 6–8). For example, TC genesis is enhanced in the SP when the MJO is active over the western Pacific and is suppressed when the MJO is over the Maritime continent reflecting the effects of active and inactive MJO phases (Ramsay *et al.*, 2012). In a localized study over the Fiji, Samoa and Tonga regions, the MJO was found to have a significant influence on TC frequency, with five times more TCs likely during the active phase compared with the inactive phase (Chand and Walsh, 2010). Chand and Walsh (2009) found that in addition to TC frequency modulation, the MJO also accounts for more severe TCs during its active phase and that TC activity gets further enhanced if the active MJO phase occurs in the El Niño years. Moreover, effects of the MJO on TC tracks is also well documented for the Southern Hemisphere basins (e.g., Chand and Walsh, 2010; Ramsay *et al.*, 2012). For example, in the South Pacific basin, TC tracks that originate from the Coral Sea tend to be steered southeastward into the Fiji and Tongan regions during MJO phases 1, 6, and 7, whereas recurved TC tracks appears more during MJO phase 8 (Chand and Walsh, 2010).

Our emphasis in this study is on TCs affecting the SI territory where the ENSO–TC relationship is not well elucidated as highlighted earlier. Better understanding of such relationship can greatly help develop strategies for preparedness and planning purposes, particularly when it comes to seasonal prediction of TCs in the region using ENSO as the main predictor (Director of SIMS, 2018, personal communication). The SI community is prone to devastating TC impacts, which often have significant socio-economic repercussions such as damages to properties and infrastructure and loss of lives (Britton, 1987). For example, prolonged torrential rainfall and flooding associated with TC *Ita* (in April 2014) had triggered a total loss of US$107.8 million, which was approximately 9.2% of the country's gross domestic product (GDP) (Solomon Islands Government, 2014). Here we examine TC characteristics over SI using a structured framework so that local-scale impacts can be better elucidated. We first objectively separate the total number of TCs observed in the SI territory over the past 50-year period into specific clusters and then explore the influence of various modes of climate variability (such as ENSO, IPO, and the MJO) on each cluster. We then develop state-of-the-art statistical models to better understand the synergistic relationship between these modes of climate variability and SI-region TC clusters. The remainder of this study is organized as follows: section 2 describes the data and methods, followed by the results and discussion in section 3. Section 4 summarizes the findings.

2 | DATA AND METHODS

2.1 | TC data and definitions

TC data are obtained from the Southwest Pacific Enhanced Archive for Tropical Cyclone (SPEArTC) online database. SPEArTC is developed using the International Best Track Archive for Climate Stewardship (IBTrACS) data primarily for the SWP region (5°–15°S, 135°E–120°W) (Diamond *et al.*, 2012). Hence, it essentially has all the qualities ascribed to IBTrACs, but with the major enhancement of the exclusion of duplicate records from various sources and the addition of tracks that were not recorded for the SPO but were archived at the Pacific Islands National Meteorological and Hydrological Services (PINMSs) (Diamond *et al.*, 2012). SPEArTC is being proven as a credible database for TC studies in the SP region (Magee *et al.*, 2016; Sharma *et al.*, 2019; Tauvale and Tsuboki, 2019). It has a 6-hourly track record since the 1840s until 2019 with a 10-min wind average as recommended by the World Meteorological Organization (WMO) (Harper *et al.*, 2008a). In this study, we only considered observations from the 1969/1970 period to coincide with the satellite era and higher-quality count data (Landsea *et al.*, 2006; Kuleshov *et al.*, 2010). We analyse seasons up to and including 2018/2019. Also, only those TCs that have achieved at least sustained wind speed of 34 knots (or ~63 $km \cdot hr^{-1}$) and have entered the SI territory (5°–15°S, 155°–170°E; Figure 1a) are considered. Using these criteria, a total of 168 TCs were recorded for the SI territory over the study period. An additional step is taken here to verify all 168 TCs with an additional data source from the Australian Bureau of Meteorology TC Data Portal (Kuleshov *et al.*, 2010; Australian Bureau of Meteorology, 2021) to ensure our records do not contain any missing or repeated tracks. Note a TC season is defined from July 1st to June 30th in the subsequent year to comply with the WMO definition for the SH which encompasses the peak cyclone season from November 1st through April 30th (e.g., Harper *et al.*, 2008a). The second calendar year is used to refer to a particular season (e.g., 1970 TC season is from July 1, 1969 to June 30, 1970).

2.2 | TC track clustering technique

The cluster technique pioneered by Gaffney (2004) was employed to assemble TC tracks into groups of similar traits. This technique comprises a mixture of polynomial regression models which can approximate each observed cyclone track into specified track regimes or "clusters"

based on TC genesis location and track shape (Gaffney, 2004). This method was effectively applied in the North Atlantic basin (Gaffney *et al*., 2007), the eastern North Pacific basin (Camargo *et al*., 2007a; 2007b), in the entire SH (Ramsay *et al*., 2012; 2018; Sharma *et al*., 2020), and the Fiji, Samoa, and Tongan region (Chand and Walsh, 2009). While methods such as *K*-means (e.g., Elsner, 2003) can also be applied in clustering of TC tracks, we prefer the model developed by Gaffney (2004) because of its ability to cluster TCs with various shapes and locations, and can handle trajectories with different lengths. A detailed explanation of the model performance and clustering technique can be found in Gaffney (2004). The underlying clustering procedures used in this study are summarized below.

Chand and Walsh (2009) showed that the second order polynomial regression model effectively described cyclone tracks in the SWP region. Here, after initial exploration of the 168 TC tracks, the second order regression function also appeared to be an ideal selection especially for goodness-of-fit over the SI region. Next, the optimal number of clusters was determined using a method developed by Gaffney (2004). This clustering method designated each cluster a log-likelihood value, which is the log-probability of occurrence of different clusters. If the probability is highest across a candidate set of clusters, then the corresponding number of clusters is selected as optimal. We found that three clusters (i.e., $k = 3$) were sufficient to capture the general characteristics of TC tracks in the SI territory (e.g., Figures 2 and 3). Because the selection of clusters can be subjective, we further explored the feasibility of $k = 2$, 4, 5, and 6 clusters. We found that clusters appear to split with the choice of higher order of clusters $k = 4$, 5, and 6, as was also reported by Chand and Walsh (2009). Consistent with other studies in the SWP (e.g., Chand and Walsh, 2009; Ramsay *et al*., 2012), our choice of $k = 3$ was found to be very stable as the results were reproducible with several different iterations.

2.3 | TC genesis position and KDE

We used the Kernel Density Estimate (KDE) (Bowman and Azzalini, 1997) to objectively determine the spatial distribution of cyclone genesis positions in the SI territory. KDE is a nonparametric method by which a density function or kernel is applied to construct a smooth probability density estimate of the observations. The constructed density estimate can then be used as a statistical representation of a larger population distribution (Figure 2). For ease of interpretation, we only showed the contours enclosing the 25, 50, and 75% of the genesis positions (Ramsay *et al*., 2012). In our study, TC genesis is defined as the first track point of each of the 168 TCs.

2.4 | ENSO modulation of SI region TCs

In this study, standardized values of the November–April Niño3.4 region (5°–5°S, 120°–170°W; e.g., Trenberth, 1997) sea surface temperature anomalies (SSTA) are utilized to define El Niño, La Niña, and the neutral years over the period 1969/1970 to 2018/2019, using 1981–2010 as the base period. El Niño and La Niña years were defined using thresholds of SSTA values of +0.5°C and above, and −0.5°C and below, respectively, in the Niño3.4 region for the duration of the TC season. Values that fall between these two thresholds were marked as ENSO neutral years. Monthly values of the Niño3.4 index are freely available at the NOAA website (NOAA/PSL, 2020). Over the 50-year period, there were 17 seasons each for El Niño and La Niña, while 16 seasons were classified as neutral phase.

We then investigated the influence of ENSO on TC frequency for the entire SI-territory (labelled "ALL") and for each of the clusters (labelled "C1," "C2," and "C3") (e.g., Figure 4). This was done by first binning each Tcyclone into their respective ENSO phases, and then calculating descriptive statistics associated with each cluster.

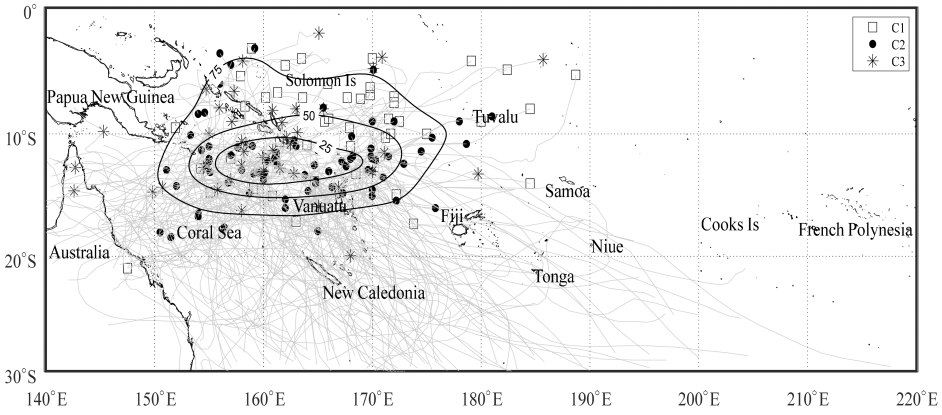

FIGURE 2 Map displaying TC genesis positions of the 168 TCs under consideration in this study. Squares, dots, and * denote genesis locations in clusters 1, 2, and 3, respectively. The grey trajectories are the observed tracks, and the contour lines represent the kernel density estimation (KDE) of all 168 genesis points at 75, 50, and 25%, respectively

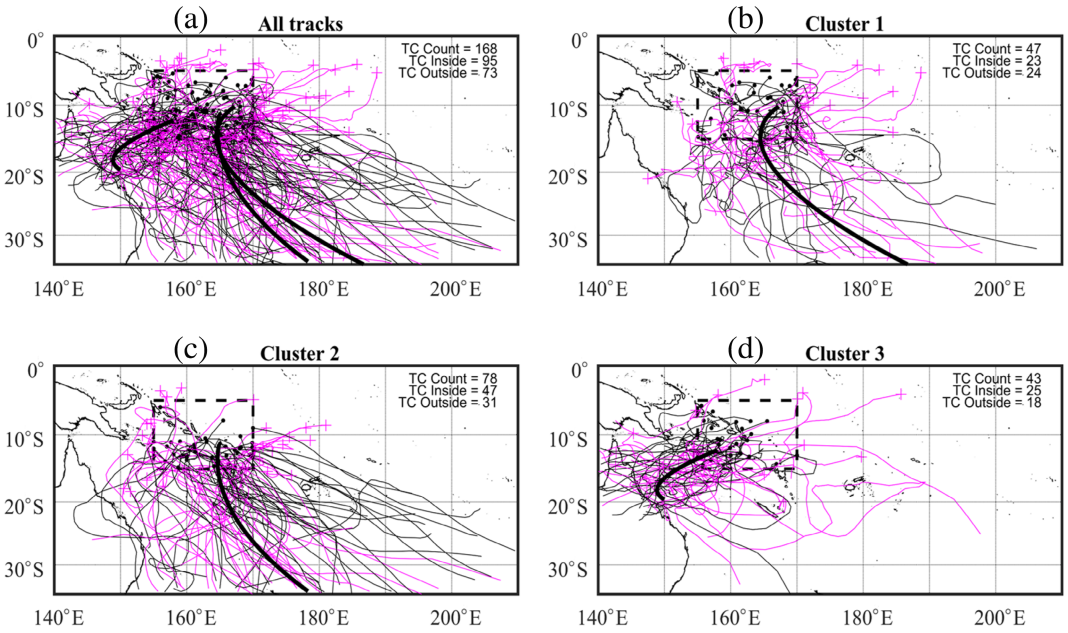

FIGURE 3 (a) ALL the 168 tracks in SI territory, and as objectively produced by the clustering approach: (b) cluster 1, (c) cluster 2, (d) cluster 3 cyclone tracks. For each panel, "TC count" signifies the total number of TCs impacting the SI region, "TC inside" represents TCs with genesis positions (dots) within the study area, and "TC outside" represents TCs that formed outside (+) and later drifted into the SI territory. The solid black curves show the mean polynomial regression trajectories for each cluster [Colour figure can be viewed at wileyonlinelibrary.com]

The conventional statistical Student's *t* test was used to establish the statistical differences in the mean TC numbers between different ENSO phases per cluster (e.g., von Storch and Zwiers, 1999).

2.5 | The MJO modulation of SI region TCs

We used the Real-Time Multivariate MJO (RMM) index that was developed by Wheeler and Hendon (2004) to investigate the MJO modulation of TC genesis in the SI territory. The index comprises a pair of empirical orthogonal functions (EOFs) derived from the 850- and 250-hPa zonal wind fields and outgoing long-wave radiation (OLR) around the equatorial region (Wheeler and Hendon, 2004). In short, the evolution of MJO across the equatorial region is described using the coefficient time series of the two EOFs known as Real-Time Multivariate MJO 1 (RMM1) and Real-Time Multivariate MJO 2 (RMM2) (Wheeler and Hendon, 2004). The index has eight MJO phases plus a weak phase (i.e., when the magnitude of RMM1 and RMM2 is less than 1). All TC analyses that involved the MJO modulations were considered only for the period 1974/1975 to 2018/2019 to coincide with the time when the MJO index became first available.

To understand the degree of the MJO modulation on TC numbers, each SI-territory TC was first stratified into one of the eight MJO phases (and the weak phase) (Figure 5a and Table 1) based on the time of TC genesis. The daily genesis rate (DGR) was then calculated for each MJO phase by dividing the total number of TCs (NTCs) in that phase with the respective total number of the MJO days (*N*); results are expressed in percentages. Then we further examined the MJO influence on TCs in each of the clusters (Figure 5b and Table 2). Note as individual bins have very few TCs, we have merged the MJO phases together into phases 2 + 3, 4 + 5, 6 + 7, 8 + 1 (and a weak phase) for ease-of-interpretation, following the categorisation by Ramsay *et al.* (2012).

The significance of TC occurrence between different MJO phases was determined using the *z*-statistical test at $\alpha = .05$ significance levels following the method applied by Hall *et al.* (2001) such that

$$z = \frac{\hat{p} - pe}{\sqrt{pe\,(1-pe)/N}}, \tag{1}$$

where z is the statistical test statistic, while $\hat{p}$ and pe are the observed and expected daily genesis rate (DGR), respectively. N represents the MJO days in each phase.

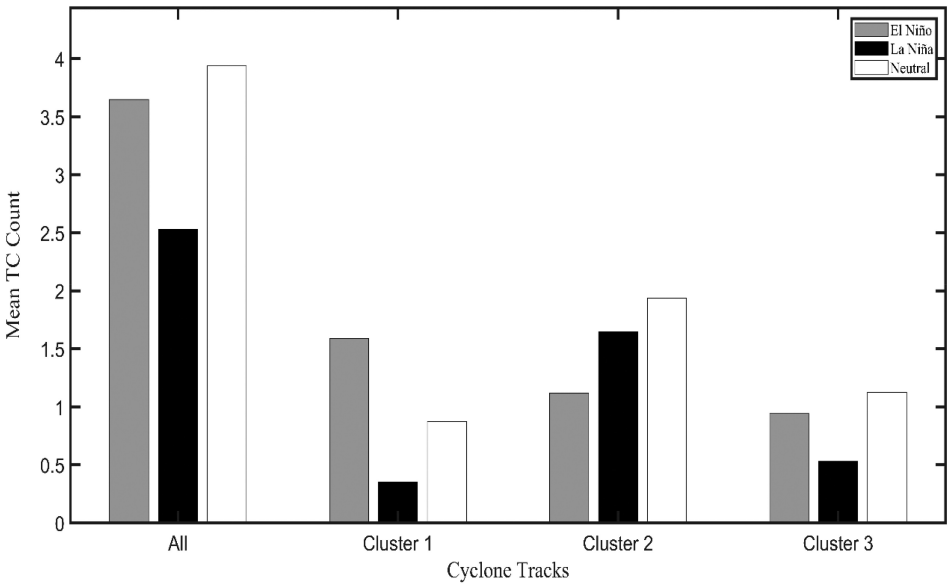

FIGURE 4 Modulation of TC counts by the three ENSO phases over the SI territory for ALL, C1, C2, and C3, respectively. Grey, black, and white bars represent modulation by El Niño, La Niña, and neutral phases, respectively

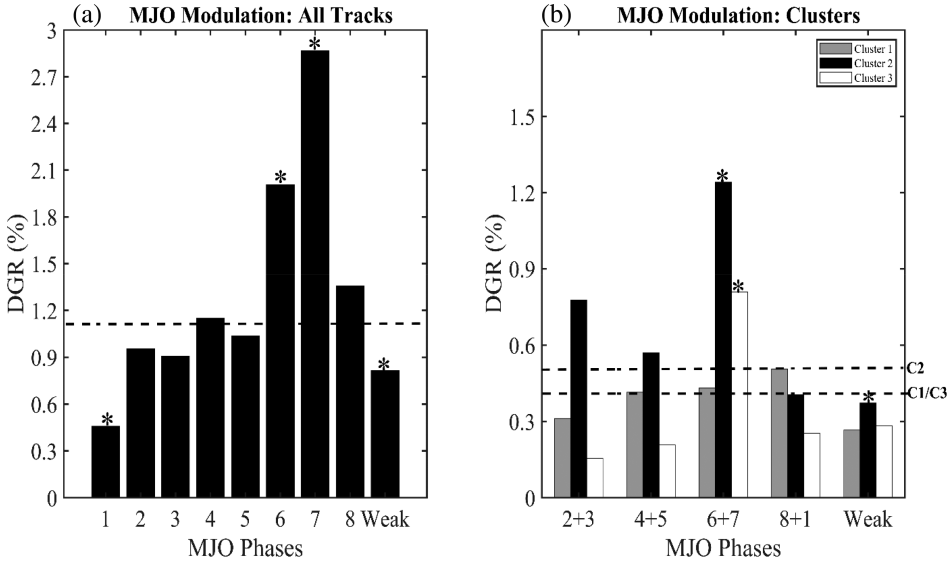

FIGURE 5 MJO modulation on TC genesis for (a) ALL TCs and (b) TCs in each cluster during 1974–2019 period in SI territory. For the later, MJO phases 2 + 3, 4 + 5, 6 + 7, 8 + 1 are combined, apart from the weak phase. Asterisk (*) indicates MJO phases that are statistically significant at the 95% confidence levels. Dashed black lines represent the expected DGR for (a) at 1.1%, and (b) at 0.5 and 0.4% for C2 and C1/C3, respectively

TABLE 1 Summary statistics for the MJO phases with the respective daily genesis rate (DGR) of observed TCs during the 1974/1975 to 2018/2019 season

MJO phases	No. of TCs in MJO phase	No. of MJO days	Daily genesis rate (%)
1	5	1,091	0.46*
2	10	1,048	0.95
3	8	883	0.91
4	10	869	1.15
5	11	1,062	1.04
6	19	947	2.01*
7	26	907	2.87*
8	12	885	1.36
Weak	46	5,645	0.81*
Total	147	13,337	1.10

Note: MJO phases that are statistically significant at 95% confidence level are indicated with asterisks (*).

MJO		Cluster 1		Cluster 2		Cluster 3	
Phase	N	NTCs	DGR	NTCs	DGR	NTC	DGR
2 + 3	1,931	6	0.31	13	0.67	3	0.16
4 + 5	1,931	7	0.36	11	0.57	3	0.16
6 + 7	1,854	6	0.32	21	1.13*	13	0.70*
8 + 1	1,976	8	0.40	8	0.40	5	0.25
Weak	5,645	9	0.16	18	0.32*	16	0.28
Total	13,337	36		71		40	

Note: N is the number of the MJO days and NTCs is the number of cyclones. MJO phases that are statistically significant at 95% confidence level are indicated with asterisks (*).

TABLE 2 Summary statistics for the MJO phases with the respective DGR for each of the clusters of observed TCs during the 1974/1975 to 2018/2019 season

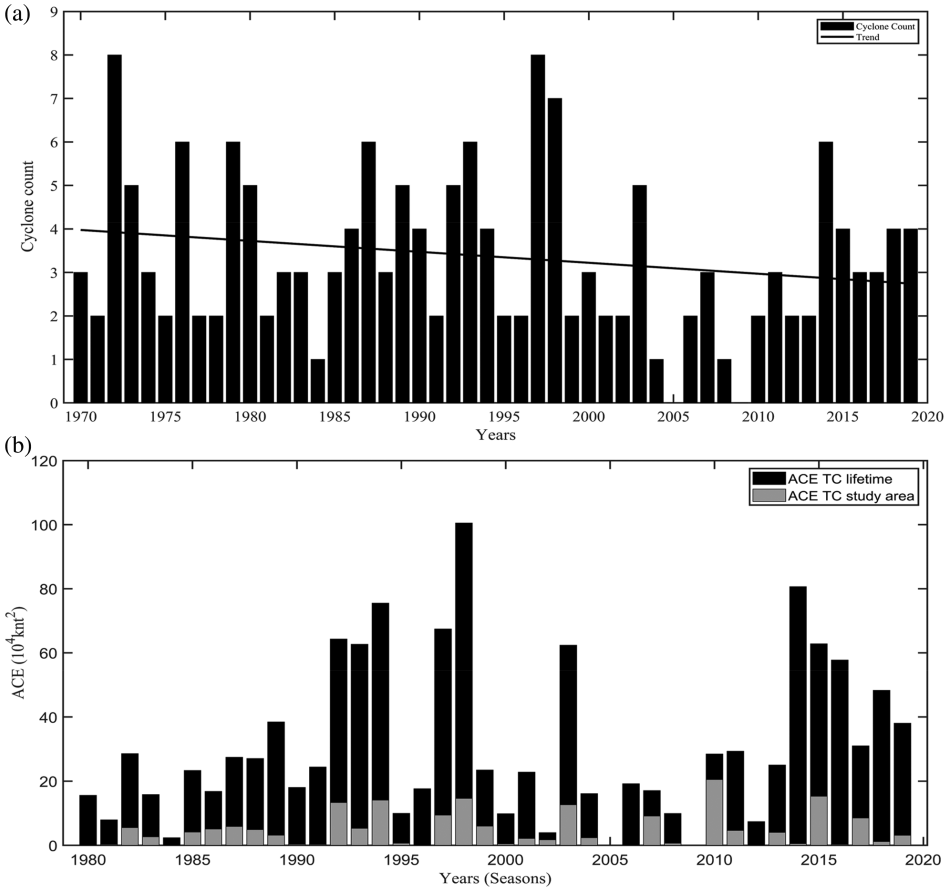

FIGURE 6 Time series for the total number of TCs (a) and ACE (b) values for the SI region from 1970 to 2019. The black line in (a) represents the linear regression fit in TC frequency. The black bars in (b) represent total ACE for each TCs lifetimes, and grey indicates fraction of ACE values only calculated over the SI region

The critical value of z at the 95% confidence levels is ±1.96 using a two-tailed test; the z-value greater (less) than the critical value of +1.96 (−1.96) is indicative of significantly enhanced (suppressed) DGR.

2.6 | TC trends analysis

We also investigated potential trends in various TC characteristics—such as seasonal TC frequency, TC days, translational speed, and accumulated cyclone energy (ACE)—over the study area. Note that because there are limited TC numbers in each of the clusters per season, the entire SI-territory observation was considered to obtain better statistical representations of these TC characteristics (Figure 6a). Here, TC frequency refers to the seasonal counts of TCs in the SI territories. We calculated TC days by first determining the lifetime of individual TCs (in days) and then accumulating them for all TCs over the season under consideration (Figure 6b). Following Kossin (2018) and Kim *et al.* (2020), the seasonal-mean translational speed is calculated by first accumulating total distances (in kilometres) between neighbouring positions along each 6-hourly TC tracks and then

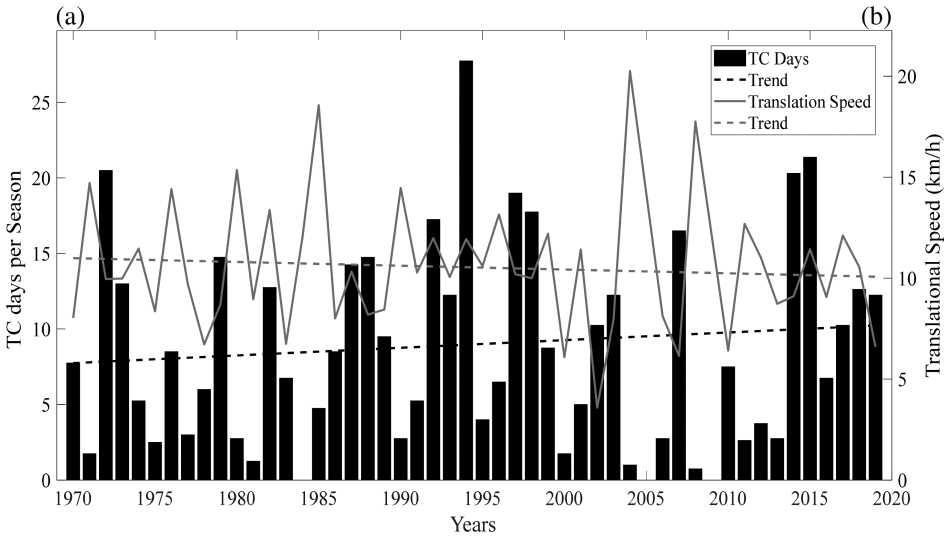

FIGURE 7 Time series for (a) TC days (black bars) with an increasing trend (black dashed line), and for (b) translational speed (grey solid line) and dashed grey line represents a decreasing trend for the SI territory during the period 1970–2019

dividing the accumulated distance by the TC lifetime (in hours) for the season under consideration (Figure 7a). Furthermore, we have computed the total seasonal ACE values for all TCs that have entered the SI territory at any point of their lifetime, as well as only for the time spent over the SI territory (e.g., Tauvale and Tsuboki, 2019) (Figure 7b). Conventionally, the annual values of ACE are obtained by computing the sum of the squares of all the estimated 6-hourly sustained wind speeds (knots) over the lifetime of a TC and finally summing the values per season such that

$$\mathrm{ACE} = \sum_{i=1}^{N} \sum_{t_i}^{t_f} v(t)^2, \tag{2}$$

where $v(t)$ is all the sustained wind speeds in knots at 6-hourly time t, t_i and t_f are the respective times of the genesis and dissipation points for each of the TC tracks, and N is the total number of TCs considered here.

2.7 | Large-scale environmental parameters and ENSO phases

Apart from modulations by the modes of natural climate variability, the connection between cyclone genesis and large-scale environmental factors is also examined for the peak months of observed TCs over the SI territory (i.e., November–April) for different ENSO phases. We used the atmospheric data from the National Centres for Environmental Protection–National Centre for Atmospheric Research (NCEP-NCAR) reanalysis model (Kalnay *et al.*, 1996). The NCEP-NCAR dataset has the horizontal resolution of 2.5° × 2.5° and is available at the NOAA Climate Prediction Centre. In the work pioneered by Gray (1979), there are pre-existing dynamical (i.e., vertical wind shear, low-level relative vorticity, and upper-level divergence) and thermodynamical (mid-level relative humidity and equivalent potential temperature) factors that are necessary for TC formation. Subsequent studies in the SWP region have revealed the significant roles played by these parameters in modulating spatial distribution of TC genesis during different ENSO (e.g., Dowdy *et al.*, 2012; Ramsay *et al.*, 2012) and the MJO phases (e.g., Camargo *et al.*, 2009; Chand and Walsh, 2010). In this study, the monthly data from 1969/1970 to 2018/2019 were extracted over the region 30°N–30°S, 60°E–60°W and utilized for computation of the most relevant factors: SST, environmental vertical wind shear (EVWS) and mid-tropospheric relative humidity (Rhum) at 700 hPa (Figures 8–10). The EVWS is defined as the magnitude of the vector difference in winds between the 200 and 850 hPa. We constructed the composites for the months of November–April for different ENSO phases to explore the spatial relationship between these factors and TC genesis positions.

2.8 | Bayesian model formulation

Finally, we developed Poisson and probit regression models using the Bayesian fitting to evaluate relationships between TC counts in each cluster and various drivers of natural climate variability that modulate them (refer to Data S1, Supporting Information for details). For the purpose of our study, the primary emphasis is the two key drivers that operate on interannual-to-decadal timescales, based on previous research findings (e.g., Mantua and Hare, 2002; Dowdy *et al.*, 2012): ENSO

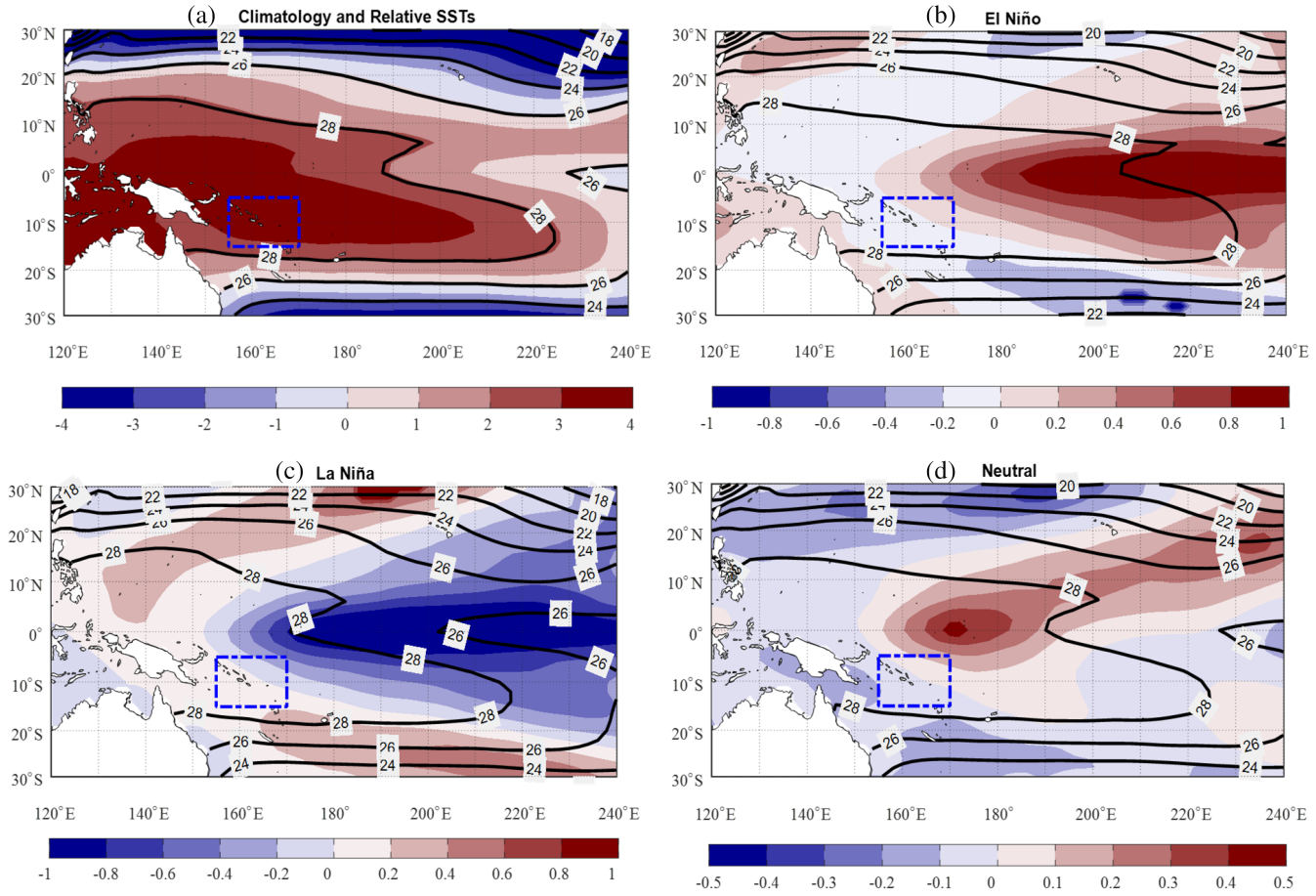

FIGURE 8 Composites of November–April SSTs (contours) and associated anomalies (shadings) over the period 1969/1970 to 2018/2019 for climatology and different ENSO phases: (a) climatology, (b) El Niño, (c) La Niña, and (d) neutral phase. Shadings in (a) represent relative SSTs defined as the difference between climatology and the tropical SST mean. SI territory is indicated with black dashed box [Colour figure can be viewed at wileyonlinelibrary.com]

and the IPO where the Niño3.4 index is used as a proxy of the conventional eastern Pacific ENSO and the Pacific Decadal Oscillation (PDO) index is used as a proxy of the IPO. Note an additional El Niño Modoki index (Ashok *et al.*, 2007) is utilized to elucidate the effects of central Pacific-type El Niño events from that of conventional ENSO on SI-territory TCs (e.g., Chand *et al.*, 2013a; 2013b). We used the standardized values of IPO and the Niño3.4 anomalies available from the NOAA website (NOAA/PSL, 2020). The EMI index is obtained from the Japanese Agency for Marine Earth Science and Technology website (JAMSTEC, 2020). Given that most of the observed TC events in the SWP and the SI territory occur from November to April (e.g., Maru *et al.*, 2018; Chand *et al.*, 2020), we only considered the mean values of these climate indices (i.e., Niño3.4, EMI, and IPO) over these 6 months period from 1970 to 2019 seasons. We developed only probit models for TCs in "C1" and "C3" because the majority of the seasons have "zeros" and "ones." The procedure is outlined in Chand and Walsh (2011a). Here, "zero" means there are no TCs, while "ones" represent if there is any (e.g., 1 or 2) TC in the cluster. For TCs in "ALL" and "C2" groups, we developed Poisson regression models following the approach by Chand *et al.* (2010) as the majority of the seasons have more than one TCs. The models take the following structures.

For the Poisson models, from equation (1) in Data S1,

$$y_i \sim \text{Poisson}\,(\lambda_i), \tag{3}$$

$$\boldsymbol{X_i} \in \{\text{Niño3.4}_i, \text{IPO}_i, \text{Modoki}_i\}; i = 1,2...,N, \tag{4}$$

$$\boldsymbol{\beta} \in \{\beta_{\text{Niño3.4}}, \beta_{\text{IPO}}, \beta_{\text{Modoki}}\},$$

$$\text{In}(\lambda_i) = \beta_0 + \boldsymbol{X_i\beta}. \tag{5}$$

And for the probit models, from equation (3) in Data S1,

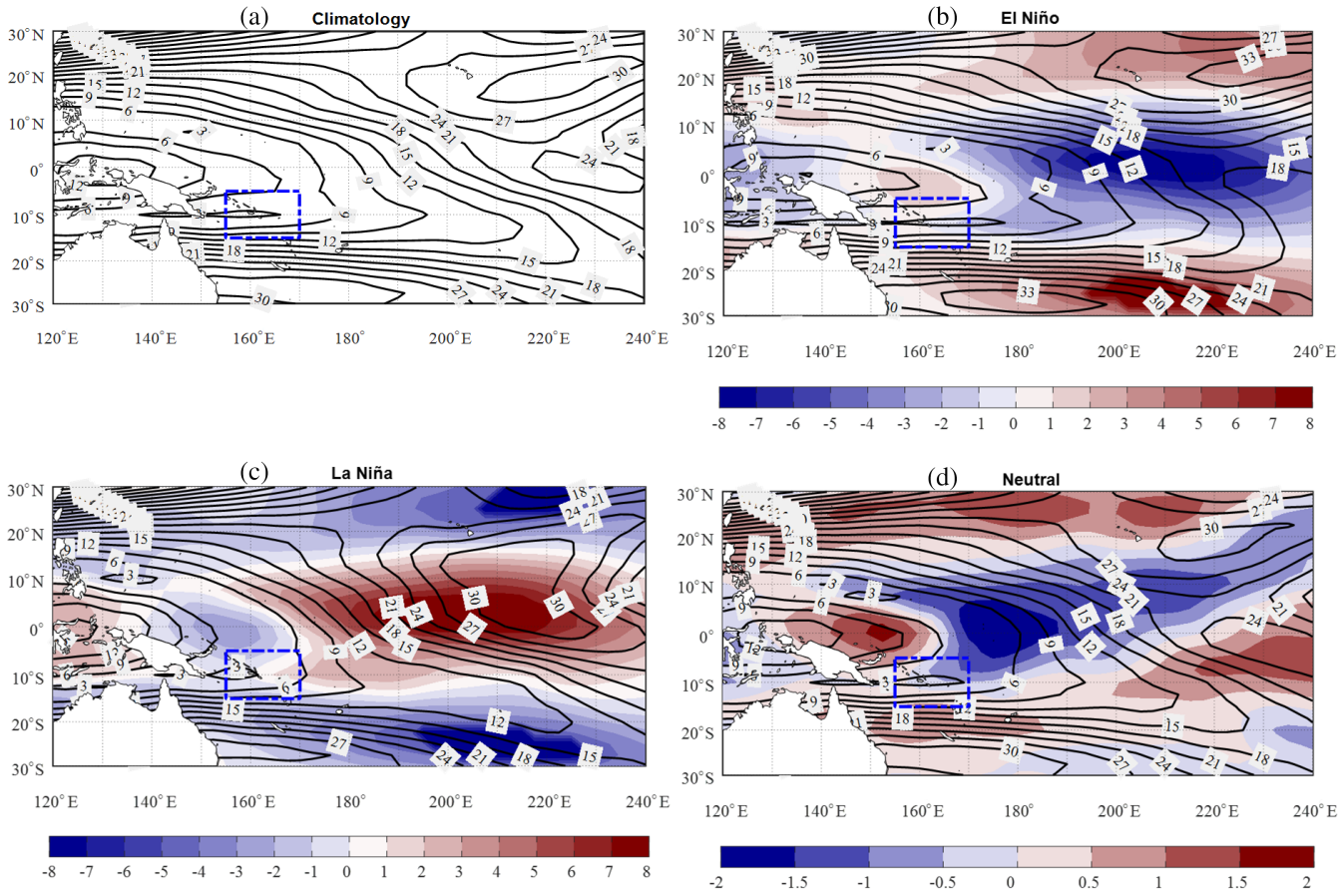

FIGURE 9 Same as Figure 8 but for environmental vertical wind shear (EVWS) between 800- and 200-hPa levels [Colour figure can be viewed at wileyonlinelibrary.com]

$$\boldsymbol{Z}_i = \boldsymbol{X_i}\boldsymbol{\beta} + \varepsilon_i, \varepsilon_i \sim N(0,1); i = 1,...,N,$$

$$\boldsymbol{X_i} \in \{1, \text{Niño3.4}_i, \text{IPO}_i, \text{Modoki}_i\}; i = 1,2...,N, \quad (6)$$

$$\boldsymbol{\beta} \in \{\beta_0, \beta_{\text{Niño3.4}}, \beta_{\text{IPO}}, \beta_{\text{Modoki}}\}, \quad (7)$$

where y_i represents the TC count per season, $\boldsymbol{Z}_i$ is an independent normally distributed latent variable vector, and ε_i is a noise vector assumed to be normally distributed with a mean of 0 and a variance of 1, $\boldsymbol{X_i}$ is the parameter vector of the related coefficient vector $\boldsymbol{\beta}$ and N is the total number of seasons (see Data S1 for details of the model formulation).

It is important to note that when applying the Bayesian approach, prior distributions must be specified for these model parameters. As such, we adopted the noninformative priors applied by Chu and Zhao (2007), which are the mean of 0 and the variance of 10^6. Because this sizeable variance represents a very little precision, it adds less information about the cyclone data.

In this study, posterior distributions of the model parameters were acquired for a total of 10,000 iterations. The WinBUGS software (Spiegelhalter *et al.*, 2002) is utilized here as it has an in-built Gibbs sampling capabilities (see Data S1 for details). To ensure the stability of the models, the initial 3,000 iterations were discarded as a "burn-in" and the subsequent 7,000 iterations were used to acquire the posterior distributions for the regression parameters. The model convergence during the first 3,000 iterations was examined through repeated sampling with different values of initial conditions. The posterior distribution of each parameter is relatively consistent for several initial conditions, indicating that the model converges to a posterior value of interest within the initial 3,000 simulations.

The posterior density distribution of the parameter coefficients related to the model is acquired using the 7,000 updates of the Gibbs sampler (see Figures 11 and 12 for the posterior density plots). The density distribution on either side of the zero mark for each parameter indicates the relative contributions of that parameter to the regression model. Any distribution

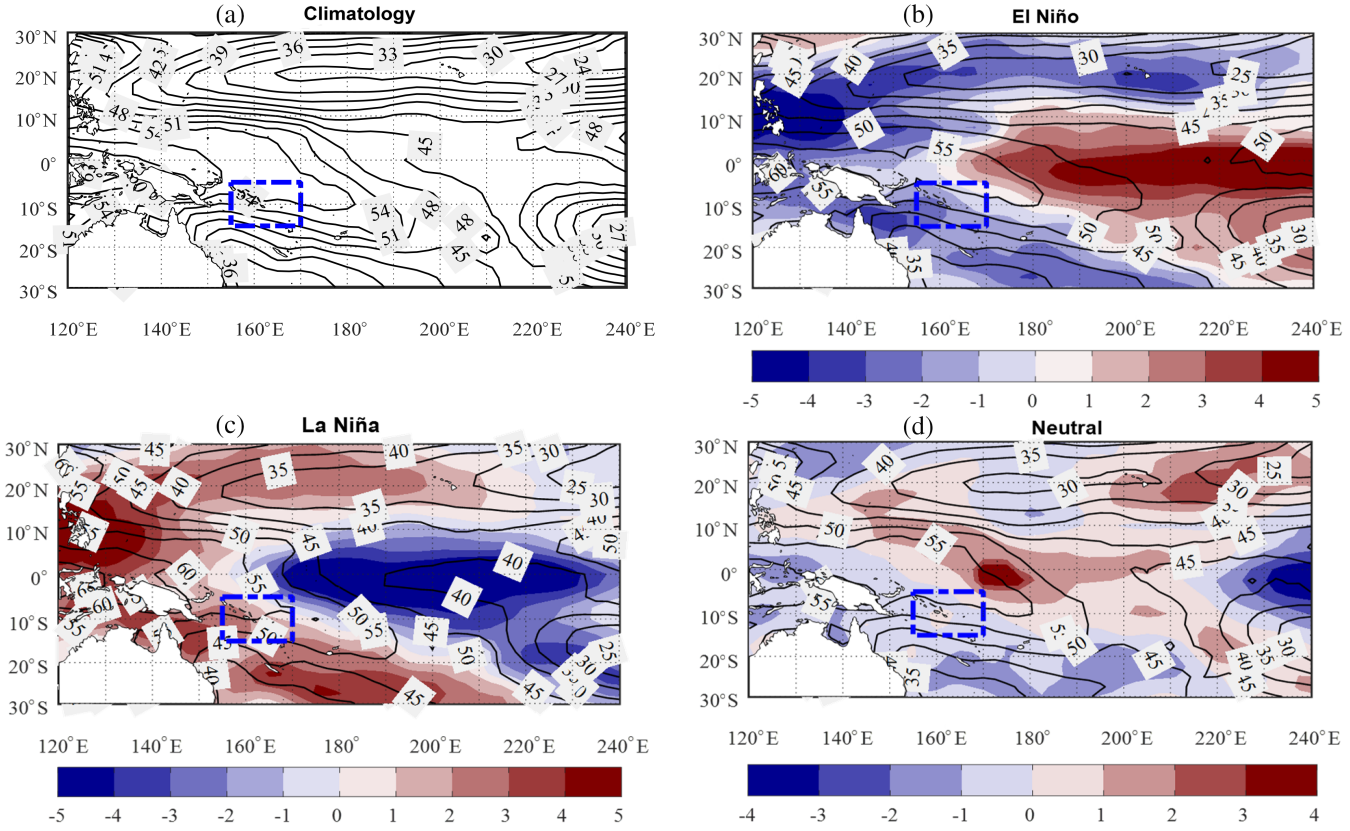

FIGURE 10 Same as Figure 8 but for mid-tropospheric relative humidity at 700-hPa levels [Colour figure can be viewed at wileyonlinelibrary.com]

where the 95% credible intervals (e.g., −0.61 and −0.21) lie outside the zero line implies that parameter significantly contributes to the model performance, whereas those that enclose the zero line have relatively low contribution towards the regression model. The autocorrelation values corresponding to the respective parameters reach zero quickly (Figure 11), signifying that the output produced by the Gibbs sampler is independently derived from their combined posterior distribution.

Using the parameters generated by the Bayesian models for each cluster, we constructed three probability matrices that can be used to make inferences when various climate variability modes co-exist. Here, we only considered the synergistic effect of Niño3.4 and IPO indices, assuming that EMI does not modulate TC formation in the SI territory as evident in Figure 13.

3 | RESULTS AND DISCUSSIONS

Research findings and discussions are organized into four parts. First part contains discussions around TC track clusters and the influence of natural climate variability on each cluster. Second part shows trends in various TC characteristics, followed by the role played by large-scale environmental factors. The final part presents the results of the Bayesian model for the SI region.

3.1 | Clustering and natural climate variability

3.1.1 | TC genesis positions

Figure 2 shows TC genesis positions of all TCs that either formed or entered the SI region over the period 1970–2019. Out of the 168 TCs under consideration, about 56% (95 TCs) formed and then drifted away or dissipated inside the study area (5°–15°S, 155°–175°E), while 44% (73 TCs) formed outside and then entered the SI territory at some point in their lifetime. Overall, the KDE contours indicate that 75% of all TCs that affected the SI region are formed between 5°–16°S and 150°–175°E, with the maximum density region (enclosed by the 25% KDE contour) between 8°–15°S and 157°–168°E. These results are consistent with that of Maru *et al.* (2018). Climatologically, some of the most severe TCs that formed in the SH since

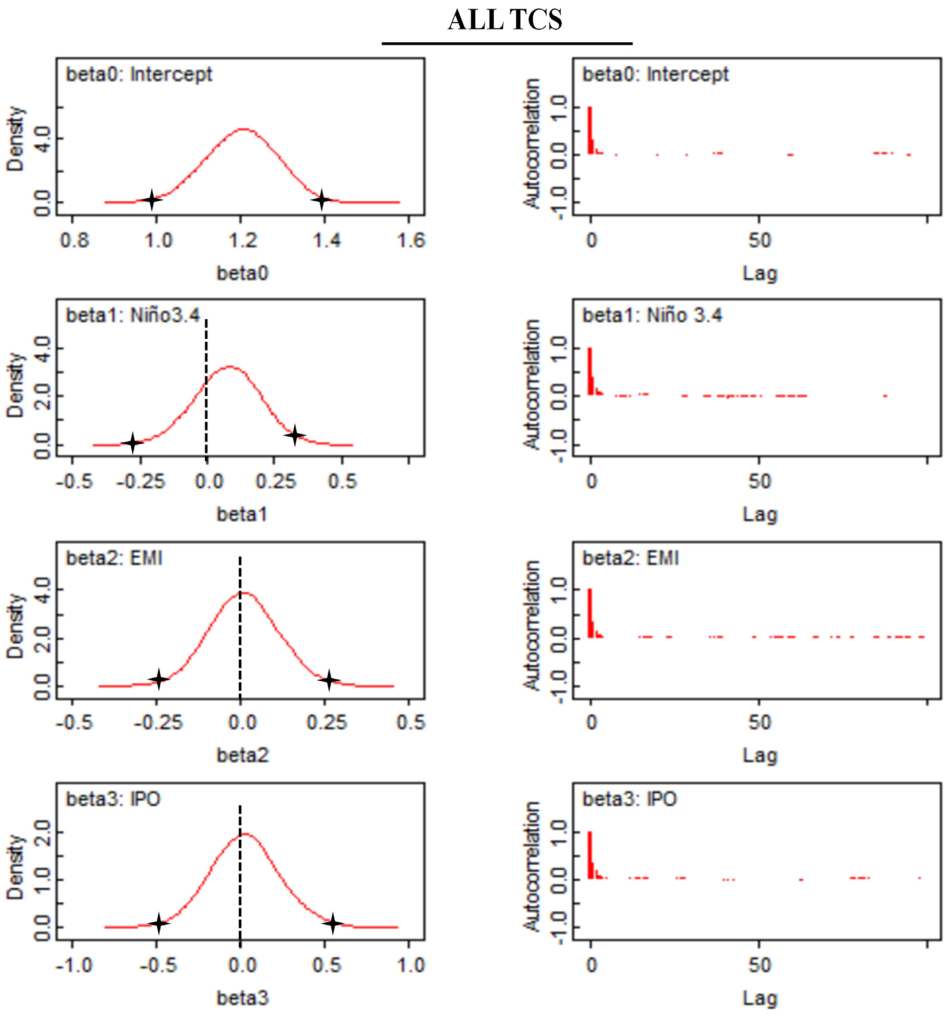

FIGURE 11 The left column presents the posterior density plots produced by the Bayesian model for each parameter (a) model intercept, (b) Niño3.4, (b) EMI, and (c) IPO for ALL TCs. The right column displays the corresponding autocorrelation plots per parameters. The vertical lines are the reference points marking "zero" positions of the distributions. The stars (*) represents the 95% credible interval [Colour figure can be viewed at wileyonlinelibrary.com]

the official records commenced had originated in this domain. For example, severe TC Winston (February 2016), originated near 6°S and 174°E and, was the most intense on record and the strongest system in the SH to make a landfall. TC Pam (March 2015, point of origin: ~9°S and 169°E), the second most intense cyclone recorded, resulted in the worst natural disaster in the history of Vanuatu. Severe TC Yasi (January 2011) was the biggest storm in the Queensland's history; it also tracked over the study area. Based on the observations, the SI region can be considered as a TC "hot spot" for TC development in the Pacific.

3.1.2 | TC track clusters

Figure 3a demonstrates the three regimes of cyclone tracks for the SI territory. Cluster 1 (C1) has a total of 47 TCs, which is ~28% of the total observation in the SI region (Figure 3b). Some tracks within C1 are very erratic during initial periods of their lifetime and appear to take arbitrary directions, as also previously documented (e.g., Holland and Gray, 1983; Terry and Gienko, 2011). In this cluster, TC formation locations are displaced equatorward to around 10°S and 170°E (Figure 3b). TCs here move southwestward initially and then "recurve" southeastward towards the Vanuatu region. The highest number of TCs belongs to cluster 2 (C2), which is about 46% (78 TCs) of the total TC observations (Figure 3c). Forty-seven of these tracks originated within the study region, then moved generally southeastward with a slight recurving trajectory into Vanuatu and Fiji territories. We note that majority of TCs that formed in the SI territory, and ultimately crossed the date line, belong to this cluster. Finally, our cluster 3 (C3) contains ~26% (43 TCs) of cyclones that recorded in the study area, mainly around 150°–169°E (Figure 3d). Unlike C1 and C2, the majority of TCs in C3 drifted westwards into the Australian region. Of all those TCs that formed outside of the SI territory (e.g., see Figure 2), the majority originated around the IDL and are associated with C1 (Figure 3b) where climatologically, as discussed later, El Niño plays a dominant role.

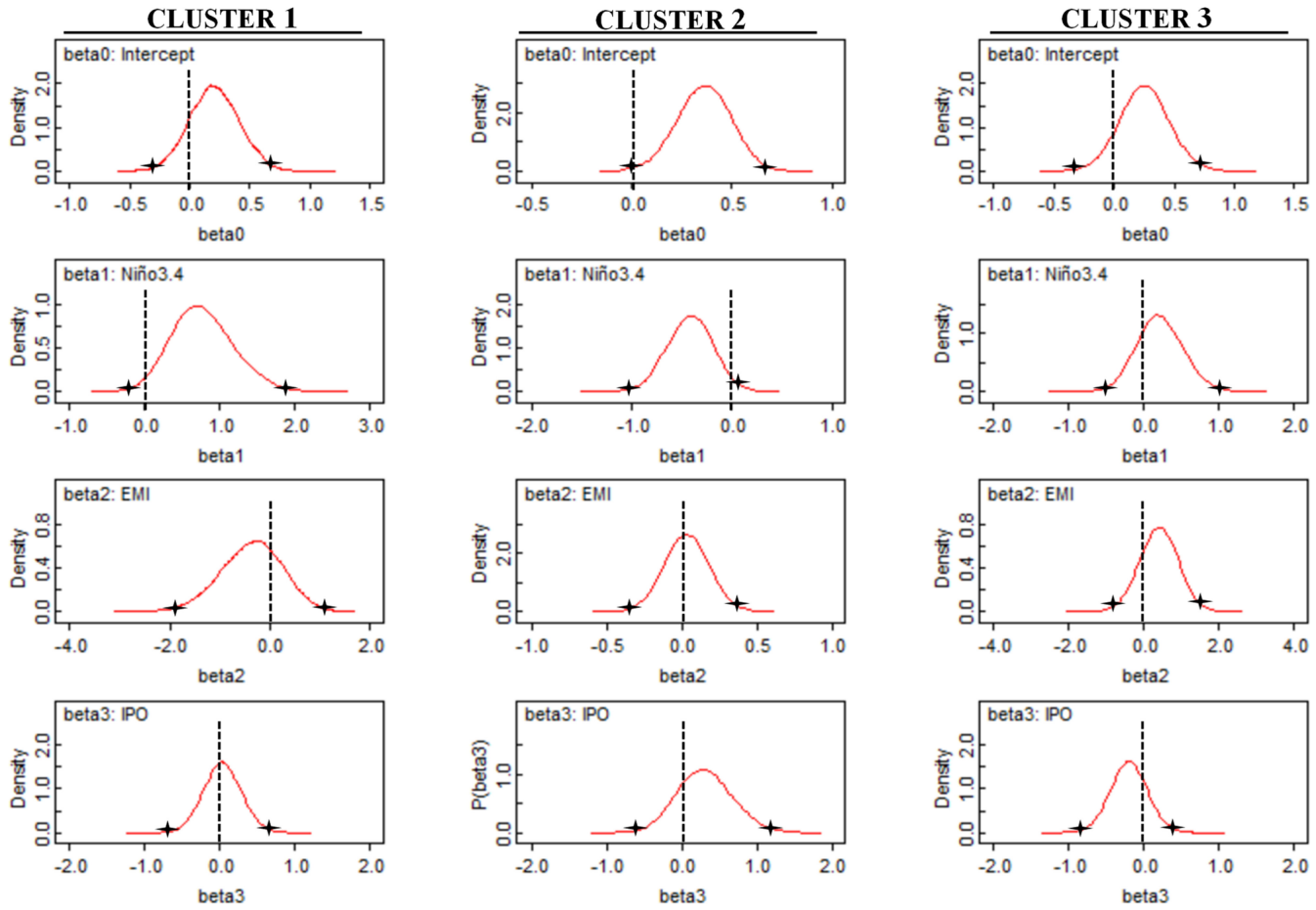

FIGURE 12 Posterior distribution plots generated by the probit models for clusters 1 and 3 (left and right columns) and Poisson model for cluster 2 (middle column). The rows denote the density plots for the *y*-intercept, Niño3.4, EMI, and IPO, respectively. The vertical lines are the reference point at "zero" position of the distributions. The stars (*) represents the 95% credible interval [Colour figure can be viewed at wileyonlinelibrary.com]

3.1.3 | Cluster-specific ENSO influences

When considering all TCs over the study area, there is a slightly higher mean annual number of TCs during El Niño and ENSO-neutral phases compared with La Niña, but these numbers are not statistically different at the 95% significance level (Figure 4, ALL). Overall, an average of ∼3.6 TCs (62 TCs), ∼2.5 TCs (43 TCs), and ∼3.9 (63 TCs) are noted in the SI territory during El Niño, La Niña, and neutral years, respectively. Climatologically, the low variability in TC numbers seen between ENSO phases is potentially because SI region is located where the ENSO phase change occurs. This demonstrates our earlier assertion (e.g., Figure 1) that the predictability of TCs in SI territory can be challenging, as opposed to TCs formed eastward towards the IDL where the ENSO influence can be more significant (Chand and Walsh, 2011b; Dowdy *et al*., 2012).

However, much clearer patterns of the ENSO–TC relationship begin to emerge when we look at each cluster separately. For C1, (i.e., which comprises TCs with recurving tracks that moved southwest initially and then drifted southeastward towards to Vanuatu region), the mean TC count is significantly higher at the 95% significance level during El Niño (∼1.6 TCs per year) than during La Niña (∼0.4 TCs per year) or neutral years (∼0.9 TCs per year) (Figure 4, cluster 1). In contrast, for C2 (Figure 4, cluster 2), mean TC count in neutral and La Niña phases (i.e., ∼1.9 and ∼1.6 TCs per year, respectively) are significantly higher than the El Niño phase which has ∼1.1 TCs per year. Interestingly, in C3 (Figure 4, cluster 3), El Niño appears to be a more prevalent phase in the regime compared with the counterpart La Niña phase. The Student's *t* test indicates that this modulation of enhanced TC activity in El Niño and neutral phases (with ∼0.9 TCs and ∼1.1 TCs per year, respectively) are statistically higher than those in La Niña (∼0.5 TCs per year). While this finding somewhat supports the conclusion that the average annual number of cyclones in the SPO (135°E–120°W) is higher during El Niño than

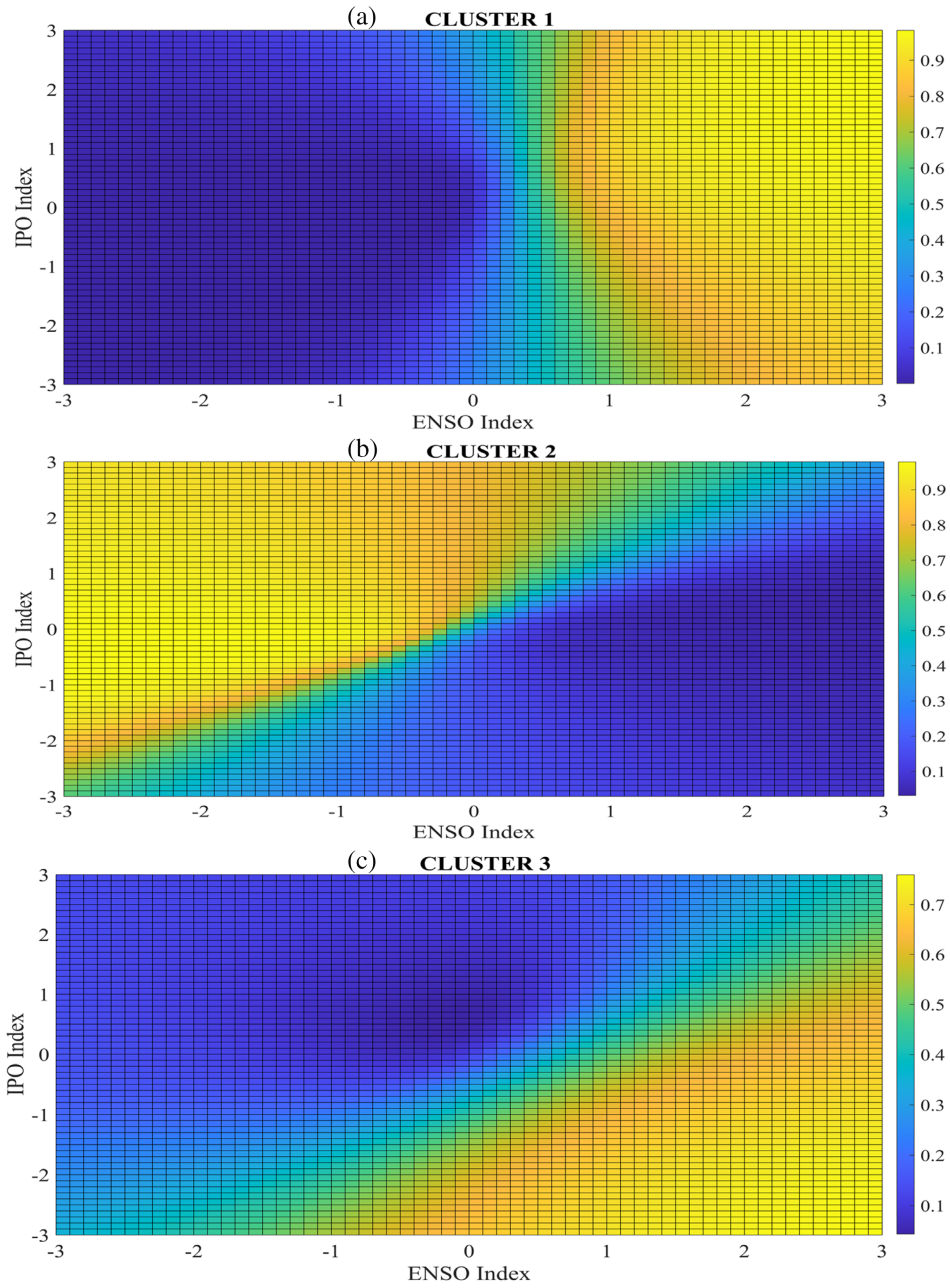

FIGURE 13 Probability distribution matrix for tropical cyclone occurrences in (a) C1, (b) C2, (c) C3 under co-existence of ENSO and IPO for the SI region [Colour figure can be viewed at wileyonlinelibrary.com]

other ENSO phases (Kuleshov *et al.*, 2020), it is also at odds with previous findings that cyclone frequency in the western section of the SWP (i.e., towards the Australia region) is greater in La Niña years when compared with El Niño years (Basher and Zheng, 1995; Chand *et al.*, 2019). However, we find here that C3 also comprises TCs that move eastward from as far as the IDL and beyond where TC formations are more prominent during El Niño than La Niña years, consistent with the finding of Dowdy *et al.* (2012). Such changes in TC numbers and genesis locations due to ENSO are linked to various large-scale environmental factors (e.g., vertical wind shear, relative humidity, and relative vorticity) that are known to influence TC occurrences in the wider SWP (Dowdy *et al.*, 2012; Ramsay *et al.*, 2012) and the SI region (Maru *et al.*, 2018).

3.1.4 | Effects of the MJO modulation

In this section, we examine effects of the MJO on TC numbers in each cluster. Figure 5a shows the daily genesis rate (DGR) of all TCs over the SI region in different MJO phases, based on the classification by Wheeler and Hendon (2004). Note that the total TCs considered is 147, as opposed to 168, as our MJO data are only from 1974 onwards to coincide with the period when the MJO index became available. Over the study period, there are

a total of 13,337 MJO days altogether, but only 147 of these days are associated with TC development. Climatologically, phase 7 shows the maximum DGR of ~2.9%, followed by the MJO phase 6 at ~2.0%. Other phases, including the weak phase, show relatively lower values of DGR (i.e., <1.5%). The two-tailed z test at the 95% significance levels indicate that TC genesis in the MJO phases 1, 6, and 7 (as well as in the weak phase) are statistically different from the climatological rate (~1.1 TCs per day) that assumes no modulation (Figure 5a and Table 1). In particular, this finding is consistent with other studies in the broader South Pacific basin (e.g., Chand and Walsh, 2010; Ramsay *et al.*, 2012; Maru *et al.*, 2018; Deo *et al.*, 2021), DGR is significantly enhanced in phases 6 and 7, which correspond to the active MJO phases over the SI region. Conversely, during inactive phases (and the weak phase), DGRs are generally lower overall, but TCs in only phase 1 and the weak phase get suppressed significantly. Climatologically, TCs are suppressed during inactive MJO phases due to less convective activity or dry weather patterns compared with active MJO phases when more convective systems often favour TC genesis (Wheeler and Hendon, 2004).

Moreover, the MJO modulations of TCs at cluster level show distinct patterns (Figure 5b and Table 2). Clearly, DGR in C2 and C3—where substantially more TCs are formed within the study area than those entering the region from the outside (e.g., Figure 3)—are significantly enhanced during the combined active MJO phases (i.e., Phase 6 + 7). The DGR in cluster 2 (cluster 3) during this active MJO phase is ~1.3 TCs per day (~0.7), as opposed to ~0.5 TCs per day (~0.3) when no modulation is assumed. TCs in other phases of the MJO are apparently not being modulated, except for the weak phase where C2 TCs are significantly suppressed. Unlike C2 and C3, we find that TCs in C1 are not being modulated at all, even during the active phases of the MJO. The reason for this is not clear, but we suspect that the MJO modulation on this El Niño-dominated cluster (e.g., Figure 4)—where more TCs enter the SI region from the east than those that form within it (e.g., Figure 3)—shifts TC genesis further northeast of the study area (e.g., Chand and Walsh, 2010), consequently, lowering TC numbers that enter the SI region.

3.2 | TC trend characteristics

Since cluster-specific TC numbers for each year are very low, statistical representation of trends can be problematic. Therefore, a decision was made to examine trend characteristics for all TCs over the entire SI region.

3.2.1 | TC frequency and ACE

The annual number of TCs in the SI region shows large year-to-year variability (Figure 6a). However, as discussed earlier, there is no clear link between the annual number of TCs in the SI region and ENSO. For example, the peak TC counts are observed for the 1972, 1997, and 1998 seasons which were a strong La Niña, a neutral, and a strong El Niño year, respectively, noting the second year is used to refer to a cyclone season. The same is true for the years of suppressed TC activity in the SI region. For example, zero TCs are noted for the seasons 2005 and 2009, which were El Niño and La Niña years, respectively. One potential reason for this is that large scale climate patterns are often not very different in any given ENSO phase over the SI region (as discussed later in section 3.3). This further strengthens the need for cluster-specific assessment of TCs in the SI region, as done in this study. Overall, we note a decreasing trend in annual TC counts for the 50-year period under consideration. This decreasing trend is consistent with other previous studies at regional and country levels (e.g., Ramsay *et al.*, 2012; Maru *et al.*, 2018; Tauvale and Tsuboki, 2019). However, it is not clear at this stage whether this trend is due to anthropogenic-induced global warming or part of long-term natural variability (Knutson *et al.*, 2020).

For the time series of ACE, we only considered the data from 1980 onwards as TC intensity estimates prior to this period can have large inconsistencies (e.g., Harper *et al.*, 2008b; Chand *et al.*, 2019). Like TC counts, annual values of ACE—computed for both, the entire TC lifetime and only for the time spent within the SI region—show a large year-to-year variability (Figure 6b), suggesting no clear trend over the study area. High annual values of ACE, such as in 1997 and 1998, expectedly coincide with the seasons of peak TC frequency. However, unlike TC counts, we find no apparent trend in the annual values of ACE over the period under consideration.

3.2.2 | TC days and translational speed

The annual number of TCs and their lifetime can be expressed using a single parameter called the TC days. This parameter can also be affected by the rate at which a TC moves (i.e., the TC translational speed). Here we examine both these parameters to get a better understanding of the time TCs spend over the SI region each year.

Overall, the annual values of TC days show a large year-to-year variability (Figure 7a). For example, the obvious peaks occur in the 1972, 1994, and 2015 seasons, coinciding with the periods of above-average TC numbers

whereas the low annual values coincide with the below-average TC numbers. Similarly, the time series for the mean TC translational speed show a large year-to-year variability in the SI region (Figure 7b). We note that the seasons with low TC translational speed generally coincide with the above-average TC days, indicating that slow-moving TCs also contribute to higher TC days, in addition to TC frequency.

There appears to be a slight (statistically insignificant) increasing trend in TC days per season over the SI region, which is somewhat inconsistent with the general conclusion of Tauvale and Tsuboki (2019) when analysing observed TCs in the greater southwest Pacific basin. We also find a weak declining trend in TC translation speed for the SI region, consistent with the findings of Kossin (2018) at the global and regional scales. Our results suggest that even though TC numbers have declined over the period 1970–2019, TC days have increased slightly over the same period, potentially linked to slower moving TCs observed in the recent years.

3.3 | Effects of large-scale environmental conditions

We assess the role of the three primary large-scale environmental factors, namely the SST (both absolute and relative), environmental vertical wind shear (EVWS), and relative humidity (Rhum) to explain the physical mechanisms that modulate TC genesis distribution in the SI region using composite analysis (Figures 8–10). Climatologically, the summertime SST in the SI region—as well as in the greater SWP from where TCs often track into the SI region—is >27°C (Figure 8a), which is well above empirical observations associated with TC formation (e.g., Gray, 1968; Tory and Dare, 2015). Figure 8a also shows the relative SST values (∼2.8–4.3°C) over the SI region and its vicinity, compared to the wider surrounding areas of the SWP. During El Niño, the region of higher SST (e.g., 27°C isotherm) is expectedly pushed farther northeast of the IDL, causing lower SST anomalies (±0.2°C) to dominate the SI region (Figure 8b). This suggests less conducive environment for TC formation in the SI region during El Niño than, for example, east of ∼170°E where SST anomalies are higher (>0.4°C). As a result, more TC tracks enter the SI region from northeast during El Niño compared with other ENSO phases (as demonstrated in C1). Conversely, during La Niña, the SST pattern reverses (Figure 8c). That is, more positive SST anomalies dominate the region west ∼170°E and the southern parts of the SI, whereas negative SST anomalies dominate the eastern region. Consequently, more cyclones form in the SI region during La Niña than El Niño events (as demonstrated in C2 and C3). The spatial distribution of SST during the neutral phase appears to be the same as for the climatology, with positive anomalies pushed north of SI around the equator (Figure 8d). Interestingly, average local SST over the SI region remains uniformly high around 29°C during all the ENSO phases than elsewhere in the wider southwest Pacific basin.

On average, the values of EVWS over the study area range from 3 to 6 $m \cdot s^{-1}$ (Figure 9a). Around the adjacent regions extending to the IDL, EVWS values are between 7 and 8 $m \cdot s^{-1}$. Eastwards of ∼160°W, as well as poleward of ∼15°S, EVWS values tend to increase substantially, and so TCs generally do not form in those regions. We found similar spatial patterns of EVWS over the SI region, and the wider SWP region, during all ENSO phases (Figure 9b–d). However, we do see relatively lower values of EVWS (hence, negative anomalies) in the region northeast of the SI region, extending farther east, during El Niño than La Niña years (Figure 9b,c). During neutral years, negative anomalies of EVWS generally dominate the SI region (Figure 9d). EVWS values from 2 to 4 $m \cdot s^{-1}$ are noted as conducive environment for TC formation in the Southern Hemisphere (Pillay and Fitchett, 2021). This may explain why more TCs move into the SI region from the northeast during El Niño compared with La Niña years as noted in cluster 1 (see also Figures 2 and 3).

Moreover, we found that the values of relative humidity are generally around 55% (Figure 10a) over the SI region, and these values do not change considerably for any of the ENSO phases (Figure 10b,c). However, during El Niño years, anomalously higher values of relative humidity are present east of ∼170°E with lower values over the SI region and west of ∼170°E (Figure 10b). The reverse occurs during La Niña (Figure 10c), suggesting less conducive environment for TC formation in the SI region during El Niño than during La Niña years. However, as discussed earlier, it is important to note that more TCs forming east of ∼170°E years can account for more cyclones entering the SI region from northeast during El Niño than other ENSO phases (as demonstrated in C1). The spatial distribution of relative humidity during the neutral phase appears to be the same as for the climatology, with positive anomalies pushed north of SI around the equator (Figure 10d).

3.4 | Bayesian models and TC predictability

3.4.1 | Posterior distribution of model parameters

We developed probit and Poisson regression models using Bayesian fittings to explain the synergistic effects of

ENSO and IPO as the key climate drivers of the annual number of TCs in the SI region. Such models can be used to assess probabilities of TC formation for cases when, one or more climatic drivers are favourable in any year. Note probit models are utilized only for clusters 1 and 3 as annual TC numbers in those clusters are very low, whereas Poisson models are used for all TCs in the SI region (labelled "ALL") and for TCs in cluster 2.

Figures 11 and 12 illustrate the posterior distribution of the model parameters associated with TCs in the entire SI region (i.e., ALL TCs) and in different clusters, respectively. Note the autocorrelations of each posterior distribution (e.g., for ALL TCs in Figure 11) reach zero fairly quickly, indicating that our time series of TC numbers are free from rapid and slowly varying changes and periodicities (i.e., stationarity assumptions are satisfied). The posterior density distributions on either side of the zero line provide insights into the relative modulation of each parameter on the annual TC numbers. For example, in cluster 1, a large proportion of the distribution of model parameters associated with "Niño 3.4" lie on the right side of the zero line (and outside the 95% credible interval), indicating that TC activity in cluster 1 is significantly enhanced during the El Niño phase (as discussed earlier, e.g., Figure 4). Similarly, in cluster 2, a large proportion of the distribution of model parameters associated "Niño3.4" lie on the left side of the zero line, indicating that TC activity in cluster 2 gets enhanced during the La Niña phase. Note for "ALL" TCs (Figure 11), such ENSO-related distribution is not very clear, hence the need for cluster-specific assessment of TCs as highlighted earlier. Unlike traditional ENSO, the Modoki ENSO seems to have no apparent effects on TCs in the SI region (as evident from the posterior distributions associated with "EMI"), except for cluster 3 where we see some indication of an enhanced TC activity during El Niño Modoki years. Similarly, we note that the effect of IPO is also not well elucidated for the SI region TCs, potentially due to the limited quantity of long-term data utilized in this study, though there is some indication that TCs in cluster 2 (cluster 3) may be enhanced during the positive (negative) phase of the IPO.

3.4.2 | Predictability of TC occurrences

TC formations in different clusters are objectively assessed using the respective probability matrix that presents the expected TC occurrences when different phases of ENSO and IPO co-exist, assuming that there is no modulation by El Niño Modoki (Figure 13). In cluster 1, we find that the probability of any TC forming is significantly enhanced (>70%) during El Niño years, as opposed to La Niña years where the probability of TC occurrence is significantly suppressed (i.e., <10%) (Figure 13a). The IPO seems to have no apparent effects on TCs in cluster 1, as discussed earlier. Similarly, we find that the chance of any TC forming in cluster 3 is predominantly enhanced (>∼60%) during the El Niño and the negative phase of the IPO (Figure 13c). In contrast, we find that the probability of the above-average TCs forming in cluster 2 is enhanced by ∼70–90% during the La Niña and the positive values of IPO. These results are consistent with our earlier findings that El Niño (La Niña) predominantly modulates TCs in C1 and C3 (C2) and the IPO seems to have moderate influence on TCs in C2 and C3.

4 | SUMMARY

We present climatological analyses of TCs affecting the SI region (i.e., 5°–15°S, 135°E–120°W) during the period 1969/1970 to 2018/2019. Altogether, 168 TCs are observed to have either formed or entered the SI region over these past five decades. Historically, the overall TC numbers in the SI region do not show any distinct pattern of variability in relation to the ENSO phenomenon. However, when objectively isolated into three specific clusters, clear patterns of the ENSO–TC relationship emerge.

TCs in clusters 1 and 3 show enhanced activity during El Niño phase, whereas TCs in cluster 2 are enhanced during La Niña and neutral phases. Cluster 1 primarily comprises cyclone tracks that move southwestward initially and then "recurve" southeastward towards the Vanuatu region. The highest number of TCs belongs to cluster 2, where the majority of tracks originated within the SI region, then moved generally southeastward with a slight recurving trajectory into Vanuatu and Fiji territories. Cluster 3 contains TCs that developed mainly around 150°–169°E, and unlike clusters 1 and 2, the majority of TCs in cluster 3 drifted westwards into the Australian region. In addition to being modulated by ENSO, TCs in clusters 2 and 3 show statistically significant modulation at the intraseasonal timescale due to the MJO phenomenon. During active phases of the MJO (i.e., phases 6 and 7), the daily genesis rate is significantly enhanced in these clusters, whereas the genesis rate is suppressed in the weak and inactive phases. Such intraseasonal variability is not apparent for TCs in cluster 1.

Over the 50-year study period, declining trends in TC frequency and mean translational speed were found, whereas TC days tends to increase over time. However, unlike TC frequency, we find no apparent trend in the annual values of ACE over the period under consideration. All these metrics demonstrate large year-to-year variability, and so it is not clear at this stage whether these trends are due to anthropogenic-induced global warming or part

of long-term natural variability. It is anticipated that as more long-term data becomes available in the future, such attributions due to global warming may be feasible.

We also developed cluster-specific regression models using the Bayesian approach to explain potential synergistic effects of ENSO and IPO on TC occurrences in the SI territory. Results indicate that while the effect of IPO is not very clear in cluster 1, TCs in clusters 2 and 3 seem to be slightly influenced by the positive and negative phases of the IPO, respectively, in addition to the substantial modulation by ENSO. These results can have substantial implications for cluster-specific development of TC prediction schemes for the SI region, which will be the focus of our subsequent study. Additionally, this study provides useful climate information for informing appropriate decision makings in the TC preparedness strategies for the SI community.

ACKNOWLEDGEMENTS

I am grateful to the Australian Government, for funding my PhD, through the Australian Award Scholarship, at Federation University Australia. Also, thanks to Evan Dekker for his guidance in MATLAB coding used for data analysis. Open access publishing facilitated by Federation University Australia, as part of the Wiley - Federation University Australia agreement via the Council of Australian University Librarians.

CONFLICT OF INTEREST

The authors declare no potential conflict of interest.

ORCID

Alick Haruhiru https://orcid.org/0000-0001-7799-5622

REFERENCES

Ashok, K., Behera, S.K., Rao, S.A. and Weng, H. (2007) El Niño Modoki and its possible teleconnection. *Journal of Geophysical Research: Oceans*, 112, 1–27. https://doi.org/10.1029/2006JC003798.

Australian Bureau of Meteorology. (2021) *Southern Hemisphere tropical cyclone data portal*. The Pacific Climate Change Science Program 2.

Basher, R.E. and Zheng, X. (1995) Tropical cyclones in the Southwest Pacific: spatial patterns and relationships to Southern Oscillation and sea surface temperature. *Journal of Climate*, 8(5), 1249–1260. https://doi.org/10.16309/j.cnki.issn.1007-1776.2003.03.004.

Bowman, A.W. and Azzalini, A. (1997) The Kernel approach with S-Plus illustrations. In: *Applied Smoothing Techniques for Data Analysis*. Oxford: Oxford University Press, p. 193.

Britton, N.R. (1987) Disaster in the South Pacific: impact of tropical cyclone "Namu" on the Solomon Islands, May 1986. *Disasters*, 11(2), 120–133.

Camargo, S.J., Robertson, A.W., Barnston, A.G. and Ghil, M. (2008) Clustering of eastern North Pacific tropical cyclone tracks: ENSO and MJO effects. *Geochemistry, Geophysics, Geosystems*, 9, 6. https://doi.org/10.1029/2007GC001861.

Camargo, S.J., Robertson, A.W., Gaffney, S.J., Smyth, P. and Ghil, M. (2007a) Cluster analysis of typhoon tracks. Part I. general properties. *Journal of Climate*, 20(14), 3635–3653. https://doi.org/10.1175/JCLI4188.1.

Camargo, S.J., Robertson, A.W., Gaffney, S.J., Smyth, P. and Ghil, M. (2007b) Cluster analysis of typhoon tracks. Part II: large-scale circulation and ENSO. *Journal of Climate*, 20(14), 3654–3676. https://doi.org/10.1175/JCLI4203.1.

Camargo, S.J., Wheeler, M.C. and Sobel, A.H. (2009) Diagnosis of the MJO modulation of tropical cyclogenesis using an empirical index. *Journal of the Atmospheric Sciences*, 66(10), 3061–3074. https://doi.org/10.1175/2009JAS3101.1.

Chan, J.C.L. (1985) Tropical cyclone activity in the Northwest Pacific in relation to the El Niño/Southern Oscillation phenomenon. *Monthly Weather Review*, 113(4), 599–606.

Chand, S. and Walsh, K. (2009) Tropical cyclone activity in the Fiji region: spatial patterns and relationship to large-scale circulation. *Journal of Climate*, 22(14), 3877–3893. https://doi.org/10.1175/2009JCLI2880.1.

Chand, S. and Walsh, K. (2010) The influence of the Madden–Julian Oscillation on tropical cyclone activity in the Fiji region. *Journal of Climate*, 23(4), 868–886. https://doi.org/10.1175/2009JCLI3316.1.

Chand, S.S., Dowdy, A., Bell, S. and Tory, K. (2020) A review of South Pacific tropical cyclones: impacts of natural climate variability and climate change. In: *Climate Change and Impacts in the Pacific*. Cham: Springer, pp. 251–273.

Chand, S.S., Dowdy, A.J., Ramsay, H.A., Walsh, K.J.E., Tory, K.J., Power, S.B., Bell, S.S., Lavender, S.L., Ye, H. and Kuleshov, Y. (2019) Review of tropical cyclones in the Australian region: climatology, variability, predictability, and trends. *Wiley Interdisciplinary Reviews: Climate Change*, 10(5), 1–17. https://doi.org/10.1002/wcc.602.

Chand, S.S., Mcbride, J.L., Tory, K.J., Wheeler, M.C., Walsh, K.J.E., McBride, L.J., Tory, J.K. and Wheeler, C.M. (2013a) Impact of different ENSO regimes on southwest pacific tropical cyclones. *Journal of Climate*, 26(2), 600–608. https://doi.org/10.1175/JCLI-D-12-00114.1.

Chand, S.S., Tory, K.J., Mcbride, J.L., Wheeler, M.C., Dare, R.A. and Walsh, K.J.E. (2013b) The different impact of positive-neutral and negative-neutral ENSO regimes on Australian tropical cyclones. *Journal of Climate*, 26(20), 8008–8016. https://doi.org/10.1175/JCLI-D-12-00769.1.

Chand, S.S. and Walsh, E.J.K. (2011a) Forecasting tropical cyclone formation in the Fiji region: a probit regression approach using Bayesian fitting. *Weather and Forecasting*, 26(2), 150–165. https://doi.org/10.1175/2010WAF2222452.1.

Chand, S.S. and Walsh, K.J.E. (2011b) Influence of ENSO on tropical cyclone intensity in the Fiji region. *Journal of Climate*, 24(15), 4096–4108. https://doi.org/10.1175/2011JCLI4178.1.

Chand, S.S., Walsh, K.J.E. and Chan, J.C.L. (2010) A Bayesian regression approach to seasonal prediction of tropical cyclones affecting the Fiji region. *Journal of Climate*, 23(13), 3425–3445. https://doi.org/10.1175/2010JCLI3521.1.

Chen, G. (2011) How does shifting Pacific Ocean warming modulate on tropical cyclone frequency over the South China Sea? *Journal of Climate*, 24(17), 4695–4700. https://doi.org/10.1175/2011JCLI4140.1.

Chen, G. and Tam, C.Y. (2010) Different impacts of two kinds of Pacific Ocean warming on tropical cyclone frequency over the

western North Pacific. *Geophysical Research Letters*, 37(1), 1–6. https://doi.org/10.1029/2009GL041708.

Choi, W., Ho, C.H., Kim, J., Kim, H.S., Feng, S. and Kang, K. (2016) A track pattern-based seasonal prediction of tropical cyclone activity over the North Atlantic. *Journal of Climate*, 29(2), 481–494. https://doi.org/10.1175/JCLI-D-15-0407.1.

Chu, P.S. and Zhao, X. (2007) A Bayesian regression approach for predicting seasonal tropical cyclone activity over central North Pacific. *Journal of Climate*, 20(15), 4002–4013. https://doi.org/10.1175/JCLI4214.1.

Deo, A., Chand, S.S., Ramsay, H., Holbrook, N.J., McGree, S., Magee, A., Bell, S., Titimaea, M., Haruhiru, A., Malsale, P., Mulitalo, S., Daphne, A., Prakash, B., Vainikolo, V. and Koshiba, S. (2021) Tropical cyclone contribution to extreme rainfall over southwest Pacific Island nations. *Climate Dynamics*, 56, 3967–3993. https://doi.org/10.1007/s00382-021-05680-5.

Diamond, H.J., Lorrey, M.A., Levinson, H.D., Lorrey, A.M., Knapp, K.R. and Levinson, D.H. (2012) Development of an enhanced tropical cyclone tracks database for the Southwest Pacific from 1840 to 2010. *International Journal of Climatology*, 32(14), 2240–2250. https://doi.org/10.1002/joc.2412.

Diamond, H.J. and Renwick, J.A. (2015) The climatological relationship between tropical cyclones in the southwest pacific and the Madden–Julian Oscillation. *International Journal of Climatology*, 686, 676–686. https://doi.org/10.1002/joc.4012.

Dowdy, A.J., Qi, L., Jones, D., Ramsay, H., Fawcett, R. and Kuleshov, Y. (2012) Tropical cyclone climatology of the South Pacific Ocean and its relationship to El Niño–Southern Oscillation. *Journal of Climate*, 25(18), 6108–6122. https://doi.org/10.1175/JCLI-D-11-00647.1.

Elsner, J.B. (2003) Tracking hurricanes. *Bulletin of the American Meteorological Society*, 84(3), 353–356. https://doi.org/10.1175/BAMS-84-3-353.

Felton, C.S., Subrahmanyam, B. and Murty, V.S.N. (2013) ENSO-modulated cyclogenesis over the Bay of Bengal. *Journal of Climate*, 26(24), 9806–9818. https://doi.org/10.1175/JCLI-D-13-00134.1.

Gaffney, S.J. (2004) *Probabilistic Curve-Aligned Clustering and Prediction with Regression Mixture Models*. California: University of California Irvine.

Gaffney, S.J., Robertson, A.W., Smyth, P., Camargo, S.J. and Ghil, M. (2007) Probabilistic clustering of extratropical cyclones using regression mixture models. *Climate Dynamics*, 29, 423–440.

Gray, W.M. (1968) Global view of the origin of tropical disturbances and storms. *Monthly Weather Review*, 96(10), 670–700.

Gray, W.M. (1979) Hirricanes: their formation, structure and likely role in the tropical circulation. In: *Meteorology over the Tropical Oceans*. Fort Collins, CO: James Glaisher House.

Hall, J.D., Matthews, A.J. and Karoly, D.J. (2001) The modulation of tropical cyclone activity in the Australian region by the Madden–Julian Oscillation. *Monthly Weather Review*, 129(12), 2970–2982. https://doi.org/10.1175/1520-0493(2001)129<2970:TMOTCA>2.0.CO;2.

Harper, B., Kepert, J. and Ginger, J. (2008a) *Guidelines for Converting between Various Wind Averaging Periods in Tropical Cyclone Conditions*. Geneva: World Meteorological Organization.

Harper, B.A., Stroud, S.A., McCormack, M. and West, S. (2008b) A review of historical tropical cyclone intensity in northwestern Australia and implications for climate change trend analysis. *Australian Meteorological Magazine*, 57(2), 121–141.

Hastings, P.A. (1990) Southern Oscillation influences on tropical cyclone activity in the Australian/South-West Pacific region. *International Journal of Climatology*, 10(3), 291–298. https://doi.org/10.1002/joc.3370100306.

Hendon, H.H. and Salby, M.L. (1994) The life cycle of the Madden–Julian Oscillation. *Journal of the Atmospheric Sciences*, 51(15), 2225–2237. https://doi.org/10.1175/1520-0469(1994)051<2225:TLCOTM>2.0.CO;2.

Hess, J.C., Elsner, J.B. and Laseur, N.E. (1995) Improving seasonal hurricane predictions for the Atlantic Basin. *Weather & Forecasting*, 10(2), 425–446. https://doi.org/10.1175/1520-0434(1995)010<0425:ishpft>2.0.co;2.

Holland, C. and Gray, W.M. (1983) *Tropical Cyclones in the Australian/Southwest Pacific Region*. Fort Collins, CO: Colorado State University. Atmospheric Science Paper 363.

Hong, C.C., Li, Y.H., Li, T. and Lee, M.Y. (2011) Impacts of central Pacific and eastern Pacific El Niños on tropical cyclone tracks over the western North Pacific. *Geophysical Research Letters*, 38(16), 1–6. https://doi.org/10.1029/2011GL048821.

JAMSTEC. (2020) *Database: El Niño Modoki*. Japan: JAMSTEC Researcher Database, pp. 1–2.

Jien, J.Y., Gough, W.A. and Butler, K. (2015) The influence of El Niño–Southern Oscillation on tropical cyclone activity in the eastern North Pacific basin. *Journal of Climate*, 28(6), 2459–2474. https://doi.org/10.1175/JCLI-D-14-00248.1.

Kalnay, E., Kanamitsu, M., Kistler, R., Collins, W., Deaven, D., Gandlin, L., Saha, S., White, G., Woollon, J. and Zhu, Y. (1996) The NCEP/NCAR 40-year reanalysis project. *Bulletin of the American Meteorological Society*, 77(3), 437–471.

Kiladis, G.N., Straub, K.H. and Haertel, P.T. (2005) Zonal and vertical structure of the Madden–Julian Oscillation. *Journal of the Atmospheric Sciences*, 62(8), 2790–2809. https://doi.org/10.1175/JAS3520.1.

Kim, H.M., Webster, P.J. and Curry, J.A. (2009) Impact of shifting patterns of pacific ocean warming on North Atlantic tropical cyclones. *Science*, 325(5936), 77–80. https://doi.org/10.1126/science.1174062.

Kim, S.H., Moon, I.J. and Chu, P.S. (2020) An increase in global trends of tropical cyclone translation speed since 1982 and its physical causes. *Environmental Research Letters*, 15(9), 094084. https://doi.org/10.1088/1748-9326/ab9e1f.

Knutson, T., Camargo, S.J., Chan, J.C.L., Emanuel, K., Ho, C.H., Kossin, J., Mohapatra, M., Satoh, M., Sugi, M., Walsh, K. and Wu, L. (2020) Tropical cyclones and climate change assessment. *Bulletin of the American Meteorological Society*, 100(10), 1987–2007. https://doi.org/10.1175/BAMS-D-18-0189.1.

Kossin, J.P. (2018) A global slowdown of tropical-cyclone translation speed. *Nature*, 558(7708), 104–107. https://doi.org/10.1038/s41586-018-0158-3.

Krishnamurthy, L., Vecchi, G.A., Msadek, R., Murakami, H., Wittenberg, A. and Zeng, F. (2016) Impact of strong ENSO on regional tropical cyclone activity in a high-resolution climate model in the North Pacific and North Atlantic Oceans. *Journal of Climate*, 29(7), 2375–2394. https://doi.org/10.1175/JCLI-D-15-0468.1.

Kuleshov, Y., Fawcett, R., Qi, L., Trewin, B., Jones, D., McBride, J. and Ramsay, H. (2010) Trends in tropical cyclones in the South Indian Ocean and the South Pacific Ocean. *Journal of*

Geophysical Research: Atmospheres, 115(1), 1–9. https://doi.org/10.1029/2009JD012372.

Kuleshov, Y., Gregory, P., Watkins, A.B. and Fawcett, R.J.B. (2020) Tropical cyclone early warnings for the regions of the Southern Hemisphere: strengthening resilience to tropical cyclones in small island developing states and least developed countries. *Natural Hazards*, 104(2), 1295–1313. https://doi.org/10.1007/s11069-020-04214-2.

Kuleshov, Y., Ming, F., Qi, L., Chouaibou, I., Hoareau, C. and Roux, F. (2009) Tropical cyclone genesis in the Southern Hemisphere and its relationship with the ENSO. *Annales Geophysicae*, 27, 2523–2538.

Landsea, C.W., Harper, B.A., Hoarau, K. and Knaff, J.A. (2006) Can we detect trends in extreme tropical cyclones ? *Science*, 313, 452–454.

Lin, I., Camargo, S.J., Patricola, C.M., Boucharel, J., Chand, S., Klotzbach, P., Chan, J.C.L., Wang, B., Chang, P., Li, T. and Jin, F. (2020) ENSO and tropical cyclones. In: McPhaden, M.J., Santoso, A. and Cai, W. (Eds.) *El Niño Southern Oscillation in a Changing Climate*. Washington, DC: American Geophysical Union, pp. 377–408.

Liu, Z., Chen, X., Sun, C., Cao, M., Wu, X. and Lu, S. (2019) Influence of ENSO events on tropical cyclone activity over the western North Pacific. *Journal of Ocean University of China*, 18(4), 784–794. https://doi.org/10.1007/s11802-019-3923-5.

Magee, A.D., Lorrey, A.M., Kiem, A.S. and Colyvas, K. (2020) A new Island-scale tropical cyclone outlook for Southwest Pacific nations and territories. *Scientific Reports*, 10(1), 1–13. https://doi.org/10.1038/s41598-020-67646-7.

Magee, A.D. and Verdon-Kidd, D.C. (2018) On the relationship between Indian Ocean sea surface temperature variability and tropical cyclogenesis in the Southwest Pacific. *International Journal of Climatology*, 38, e774–e795. https://doi.org/10.1002/joc.5406.

Magee, A.D., Verdon-Kidd, D.C., Diamond, H.J. and Kiem, A.S. (2017) Influence of ENSO, ENSO Modoki, and the IPO on tropical cyclogenesis: a spatial analysis of the Southwest Pacific region. *International Journal of Climatology*, 37, 1118–1137. https://doi.org/10.1002/joc.5070.

Magee, A.D., Verdon-Kidd, D.C. and Kiem, A.S. (2016) An intercomparison of tropical cyclone best-track products for the Southwest Pacific. *Natural Hazards and Earth System Sciences*, 16(6), 1431–1447. https://doi.org/10.5194/nhess-16-1431-2016.

Mantua, N.J. and Hare, S.R. (2002) The Pacific Decadal Oscillation. *Journal of Oceanography*, 58(1), 35–44. https://doi.org/10.1023/A:1015820616384.

Mantua, N.J., Hare, S.R., Zhang, Y., Wallace, J.M. and Francis, R.C. (1997) A Pacific Interdecadal climate oscillation with impacts on Salmon production. *Bulletin of the American Meteorological Society*, 78(6), 1069–1079. https://doi.org/10.1175/1520-0477(1997)078<1069:APICOW>2.0.CO;2.

Maru, E., Shibata, T. and Ito, K. (2018) Statistical analysis of tropical cyclones in the Solomon Islands. *Atmosphere*, 9(6), 1–13. https://doi.org/10.3390/atmos9060227.

Newman, M., Alexander, M.A., Ault, T.R., Cobb, K.M., Deser, C., Di Lorenzo, E., Mantua, N.J., Miller, A.J., Minobe, S., Nakamura, H., Schneider, N., Vimont, D.J., Phillips, A.S., Scott, J.D. and Smith, C.A. (2016) The Pacific Decadal Oscillation, revisited. *Journal of Climate*, 29(12), 4399–4427. https://doi.org/10.1175/JCLI-D-15-0508.1.

NOAA/PSL. (2020) *Niño 3.4 SST Index*. NOAA Working Group on Surface Pressure, pp. 1–4.

Patricola, C.M., Camargo, S.J., Klotzbach, P.J., Saravanan, R. and Chang, P. (2018) The influence of ENSO flavors on western North Pacific tropical cyclone activity. *Journal of Climate*, 31(14), 5395–5416. https://doi.org/10.1175/JCLI-D-17-0678.1.

Pillay, M.T. and Fitchett, J.M. (2021) On the conditions of formation of Southern Hemisphere tropical cyclones. *Weather and Climate Extremes*, 34, 100376. https://doi.org/10.1016/j.wace.2021.100376.

Ramsay, H. (2017) The global climatology of tropical cyclones. In: *Oxford Research Encyclopedia of Natural Hazard Science*. USA: Oxford University Press.

Ramsay, H.A., Camargo, S.J. and Kim, D. (2012) Cluster analysis of tropical cyclone tracks in the Southern Hemisphere. *Climate Dynamics*, 39(3), 897–917. https://doi.org/10.1007/s00382-011-1225-8.

Ramsay, H.A., Chand, S.S. and Camargo, S.J. (2018) A statistical assessment of Southern Hemisphere tropical cyclone tracks in climate models. *Journal of Climate*, 31(24), 10081–10104. https://doi.org/10.1175/JCLI-D-18-0377.1.

Ramsay, H.A., Richman, M.B. and Leslie, L.M. (2014) Seasonal tropical cyclone predictions using optimized combinations of ENSO regions: application to the coral sea basin. *Journal of Climate*, 27(22), 8527–8542. https://doi.org/10.1175/JCLI-D-14-00017.1.

Salinger, M.J., Renwick, J.A. and Mullan, A.B. (2001) Interdecadal Pacific Oscillation and South Pacific. *International Journal of Climatology*, 1721, 1705–1721.

Sharma, K.K., Magee, A.D. and Verdon-Kidd, D.C. (2020) Variability of Southwest Pacific tropical cyclone track geometry over the last 70 years. *International Journal of Climatology*, 41, 529–546. https://doi.org/10.1002/joc.6636.

Sharma, K.K., Verdon-Kidd, D.C. and Magee, A.D. (2019) Decadal variability of tropical cyclogenesis and decay in the Southwest Pacific. *International Journal of Climatology*, 40(5), 2811–2829. https://doi.org/10.1002/joc.6368.

Solomon Islands Government. (2014) *Solomon Islands: Rapid Assessment of the Macro and Sectoral Impacts of Flash Floods in the Solomon Islands, April 2014*. Washington, DC: World Bank.

Spiegelhalter, D.J., Best, N.G., Carlin, B.P. and Van Der Linde, A. (2002) Bayesian measures of model complexity and fit. *Journal of the Royal Statistical Society. Series B: Statistical Methodology*, 64(4), 583–616. https://doi.org/10.1111/1467-9868.00353.

Tauvale, L. and Tsuboki, K. (2019) Characteristics of tropical cyclones in the Southwest Pacific. *Journal of the Meteorological Society of Japan*, 97(3), 711–731. https://doi.org/10.2151/jmsj.2019-042.

Terry, J.P. and Gienko, G. (2011) Developing a new sinuosity index for cyclone tracks in the tropical South Pacific. *Natural Hazards*, 59(2), 1161–1174. https://doi.org/10.1007/s11069-011-9827-3.

Tory, K.J. and Dare, R.A. (2015) Sea surface temperature thresholds for tropical cyclone formation. *Journal of Climate*, 28(20), 8171–8183. https://doi.org/10.1175/JCLI-D-14-00637.1.

Trenberth, K.E. (1997) The definition of El Niño. *Bulletin of the American Meteorological Society*, 78(12), 2771–2777. https://doi.org/10.1175/1520-0477(1997)078<2771:TDOENO>2.0.CO;2.

Vincent, D.G. (1994) The South Pacific convergence zone (SPCZ): a review. *Monthly Weather Review*, 122(9), 1949–1970. https://doi.org/10.1175/1520-0493(1994)122<1949:TSPCZA>2.0.CO;2.

Vincent, M.E., Lengaigne, M.M., Christophe, E., Nicolas, C.J., Marchesiello, P. and Gurvan, M. (2011) Interannual variability of the South Pacific Convergence Zone and implications for tropical cyclone genesis. *Climate Dynamics*, 36, 1881–1896.

von Storch, H. and Zwiers, F.W. (1999) Statistical analysis in climate research. In: *Statistical Analysis in Climate Research*. Cambridge: Cambridge University Press, p. 484.

Wheeler, M.C. and Hendon, H.H. (2004) An all-season Real-Time Multivariate MJO Index: development of an index for monitoring and prediction. *Monthly Weather Review*, 132(8), 1917–1932. https://doi.org/10.1175/1520-0493(2004)132<1917:AARMMI>2.0.CO;2.

Widlansky, M.J., Webster, P.J. and Hoyos, C.D. (2011) On the location and orientation of the South Pacific Convergence Zone. *Climate Dynamics*, 36(3), 561–578. https://doi.org/10.1007/s00382-010-0871-6.

Zhang, C. (2005) Madden–Julian Oscillation. *Reviews of Geophysics*, 43, RG2003. https://doi.org/10.1029/2004RG000158.1.

Zhang, C. (2013) Madden–Julian Oscillation: bridging weather and climate. *Bulletin of the American Meteorological Society*, 94(12), 1849–1870. https://doi.org/10.1175/BAMS-D-12-00026.1.

Zhang, Y., Wallace, J.M. and Battisti, D.S. (1997) ENSO-like interdecadal variability: 1900–93. *Journal of Climate*, 10(5), 1004–1020. https://doi.org/10.1175/1520-0442(1997)010<1004:eliv>2.0.co;2.

SUPPORTING INFORMATION

Additional supporting information can be found online in the Supporting Information section at the end of this article.

How to cite this article: Haruhiru, A., Chand, S. S., Turville, C., & Ramsay, H. (2023). Tropical cyclone activity in the Solomon Islands region: Climatology, variability, and trends. *International Journal of Climatology*, *43*(1), 593–614. https://doi.org/10.1002/joc.7797